Fluid Phase Equilibria 577 (2024) 113961

Contents lists available at ScienceDirect

Fluid Phase Equilibria

journal homepage: www.journals.elsevier.com/fluid-phase-equilibria

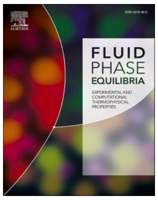

Liquid−vapor order parameter and coexistence-curve diameter of nitrogen, ethylene, and sulfur hexafluoride: From the triple point to the critical scaling regime

Roman Tomaschitz

Sechsschimmelgasse 1/21-22, Vienna A-1090, Austria

ARTICLE INFO

Keywords:
Coexistence-curve diameter
Order parameter
Vapor−liquid equilibria
Critical power-law scaling
Effective exponents
Nonlinear least-squares regression

ABSTRACT

Analytic closed-form expressions are obtained for the liquid and vapor saturation densities defining the coexistence curve. The densities are modeled with broken power laws and Weibull distributions. Specifically, the coexistence curves of nitrogen, ethene and sulfur hexafluoride are derived, without the use of perturbative expansions, based on high-precision data extending from the triple point into the critical regime. The analytic continuation of the vapor branch below the triple point decays exponentially at low temperature. The order parameter and coexistence-curve diameter of the fluids are assembled from the regressed liquid and vapor branches of the coexistence curve, and the critical power-law scaling of these quantities is examined. The scaling exponents of the order parameter and the reduced diameter are regressed and compared with the calculated critical exponents of the 3D Ising universality class. Index functions representing the Log−Log slopes (temperature-dependent effective exponents) of the liquid and vapor densities, order parameter and diameter are used to determine the onset of the ideal power-law scaling regime and to illustrate the slope evolution of these quantities in the subcritical regime.

1. Introduction

The aim of this paper is to model the coexistence curve of molecular one-component fluids empirically, over the entire temperature range from the triple point to the critical point, based on experimental data sets only, cf. Refs. [1–3], without calculated input from critical scaling theory. We will obtain the liquid and vapor branches of the coexistence curve in closed analytic form by nonlinear least-squares regression of multiparameter distributions composed of broken power-law densities and Weibull exponentials.

As for the critical scaling regime, the data sets used extend into the $|1 - T/T_c| < 10^{-3}$ interval (T_c denoting the critical temperature), which makes it possible to extract the scaling exponent β of the coexistence curve empirically, without resorting to the calculated 3D Ising exponent as predetermined input. This is also warranted by the fact that there have been two independent measurements of β in binary mixtures [4,5], where deviations of about 12 % from the 3D Ising value $\beta = 0.3264$, cf. Ref. [6], were reported. In coexistence-curve measurements of liquid alkali metals, β exponents of 0.355 ± 0.01 for Cs and 0.360 ± 0.01 for Rb have been found in Ref. [7], also largely exceeding the 3D Ising exponent.

We will derive the coexistence curve of three fluids, nitrogen (N_2), ethylene (C_2H_4) and sulfur hexafluoride (SF_6), for which high-precision data sets are available from the critical regime to the triple point, cf. Refs. [1–3,8–11]. The order parameter and coexistence-curve diameter can be assembled from the regressed liquid and vapor branches, and we will discuss the critical scaling of these quantities and especially their temperature evolution beyond the critical regime, which covers only a tiny fraction of the data range. Critical scaling predictions such as the putative $|1 - T/T_c|^{2\beta}$ scaling of the reduced coexistence-curve diameter, cf. Refs. [3,7,12–21], can be tested by means of Index functions (effective exponents), cf. Refs. [22–26], representing the temperature-dependent Log−Log slope of the coexistence curve, order parameter and reduced diameter. The Log−Log slope of these quantities becomes asymptotically constant in the power-law scaling regime, with the respective scaling exponent as limit value.

In Section 2, the relations between the liquid and vapor branches of the coexistence curve and the order parameter and coexistence-curve diameter are outlined and illustrated with the corresponding data sets for nitrogen. We will briefly sketch the critical power-law scaling of the coexistence curve, which is parametrized by reduced temperature $t = 1 - T/T_c$, and the critical scaling of the order parameter.

E-mail address: tom@geminga.org.

https://doi.org/10.1016/j.fluid.2023.113961
Received 12 May 2023; Received in revised form 12 September 2023; Accepted 29 September 2023

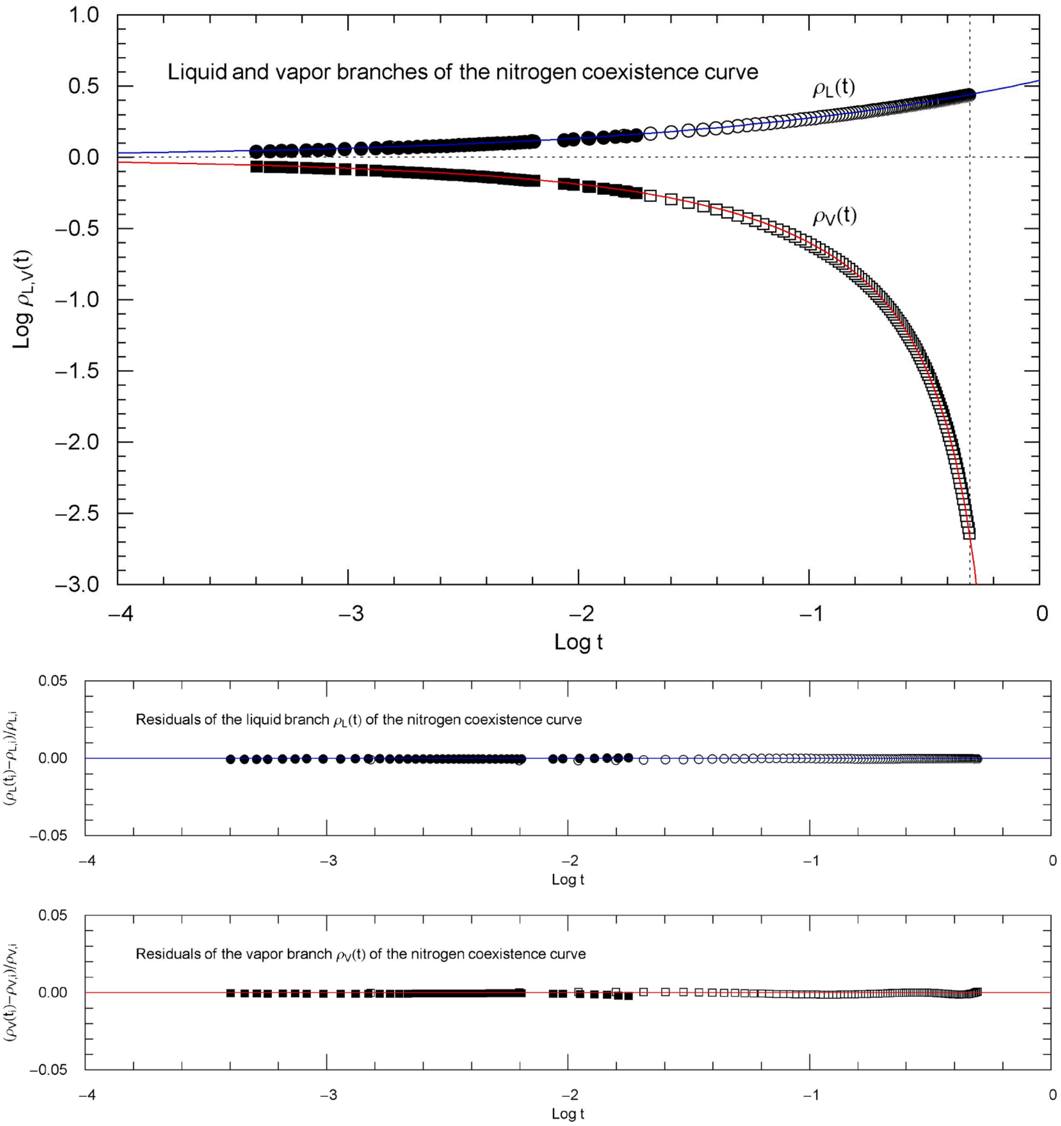

Fig. 1. Coexistence curve of nitrogen. Depicted are the liquid and vapor branches $\rho_L(t)$ and $\rho_V(t)$ of the coexistence curve in double-logarithmic representation, parametrized with reduced temperature, cf. Sections 2 and 5. The data sets are from Ref. [3] (filled symbols) and Refs. [1,2] (open symbols). The vertical dotted line indicates the triple-point temperature, cf. Table 1. The blue and red solid curves show the regressed branches $\rho_L(t)$ and $\rho_V(t)$ in (3.1) and (3.2), with fitting parameters in Tables 2 and 3. The vapor branch $\rho_V(t)$ decays exponentially. Residual plots of the regressed branches are shown in the lower panels, indicating relative deviations from the data points of less than one percent.

In Section 3.1, the closed-form representation of the liquid and vapor branches of the coexistence curve will be specified. A Weibull-type exponential is used for the vapor density, which remains stable below the triple point and decays exponentially for $t \to 1$, i.e. in the zero-temperature limit. The liquid branch of the coexistence curve is modeled with a linear combination of a broken power law and a Weibull exponential, the broken power-law density being a substitute for the rectilinear diameter rule, cf. Refs. [7,12,14,15]; the latter gives a reasonably accurate approximation of the coexistence-curve diameter of molecular fluids, except in the critical regime.

The least-squares regression of the coexistence curve is explained in Section 3.2, in particular the nonlinear χ^2 functional to be minimized in the regression. A simultaneous fit of the liquid and vapor branches is required, since they have several parameters in common, such as the scaling exponents of the order parameter and reduced diameter. Goodness-of-fit parameters and the covariance matrix for the estimation of error bounds on the regressed parameters are outlined as well.

In Section 4, Index functions (temperature-dependent effective exponents) defined by the Log−Log slope of the coexistence-curve branches, order parameter and diameter will be discussed. Power laws appear as straight lines in Log−Log plots, with the power-law index as constant slope parameter. Index functions generalize this, describing the Log–Log slope evolution of arbitrary densities. In the case of the coexistence curve, the local Log–Log slope depends on reduced temperature, and the varying Index function (effective exponent) admits a constant limit value in the critical scaling regime, which coincides with the scaling exponent. Index functions will be used to locate the power-law scaling regime, where they are nearly constant, and to depict slope evolution of the reduced liquid and vapor densities, order parameter and diameter beyond the critical regime.

In Section 5, we will regress the coexistence curves of nitrogen, ethylene and sulfur hexafluoride, based on data sets from Refs. [1–3]. The data from Refs. [1,2] are synthetic, provided in machine-readable form and derived from multiparameter equations of state obtained from a variety of data sources, cf. Refs. [8–11]. Residual plots will be used to depict the local percentage deviation of the data points from the

Table 1

Critical constants (temperature T_c, molar density ρ_c, molar volume $V_\mathrm{c} = 1/\rho_\mathrm{c}$, pressure P_c) and triple-point temperature T_tr of nitrogen (N_2), ethylene (ethene, C_2H_4), and sulfur hexafluoride (SF_6), cf. Refs. [1,2].

	T_c[K]	ρ_c[mol /cm^3]	V_c[cm^3 /mol]	P_c[MPa]	T_tr[K]
N_2	126.19	0.011184	89.414	3.3958	63.15
C_2H_4	282.35	0.007637	130.94	5.0418	103.986
SF_6	318.723	0.0050823	196.76	3.75498	223.555

regressed liquid and vapor branches of the coexistence curve. These deviations are well below one percent over the entire data range. For each fluid, we will extract the critical scaling exponents of the order parameter and reduced diameter and compare them with the calculated exponents of the 3D Ising model. The Index functions of the reduced liquid and vapor densities, order parameter and reduced diameter will be calculated for each fluid, in this way quantifying the crossover from the ideal power-law scaling regime to the experimentally more accessible low-temperature range above the triple point. Section 5 also contains the discussion of the above outlined results, and Section 6 summarizes the conclusions.

2. Coexistence curve, order parameter, and coexistence-curve diameter

The liquid and vapor branches of the molar density along the coexistence curve are denoted by $\rho_\mathrm{L}(t)$, $\rho_\mathrm{V}(t)$. They are parametrized with reduced temperature $t = 1 - T/T_\mathrm{c}$ and normalized with the critical density ρ_c to make them dimensionless, so that $\rho_\mathrm{L}(t = 0) = \rho_\mathrm{V}(t = 0) = 1$ at the critical point. The critical-point constants (temperature, molar density, pressure, molar volume) are labeled $T_\mathrm{c}, \rho_\mathrm{c}, P_\mathrm{c}, V_\mathrm{c} = 1/\rho_\mathrm{c}$. The temperature varies in the subcritical interval $T_\mathrm{tr} \le T \le T_\mathrm{c}$, where T_tr denotes the triple-point temperature.

Fig. 1 shows, as a first orientation, a plot the data points $(t_i, \rho_{\mathrm{L},i})_{i=1,\ldots,N}$ and $(t_i, \rho_{\mathrm{V},i})_{i=1,\ldots,N}$ in decadic Log–Log coordinates, defining the vapor

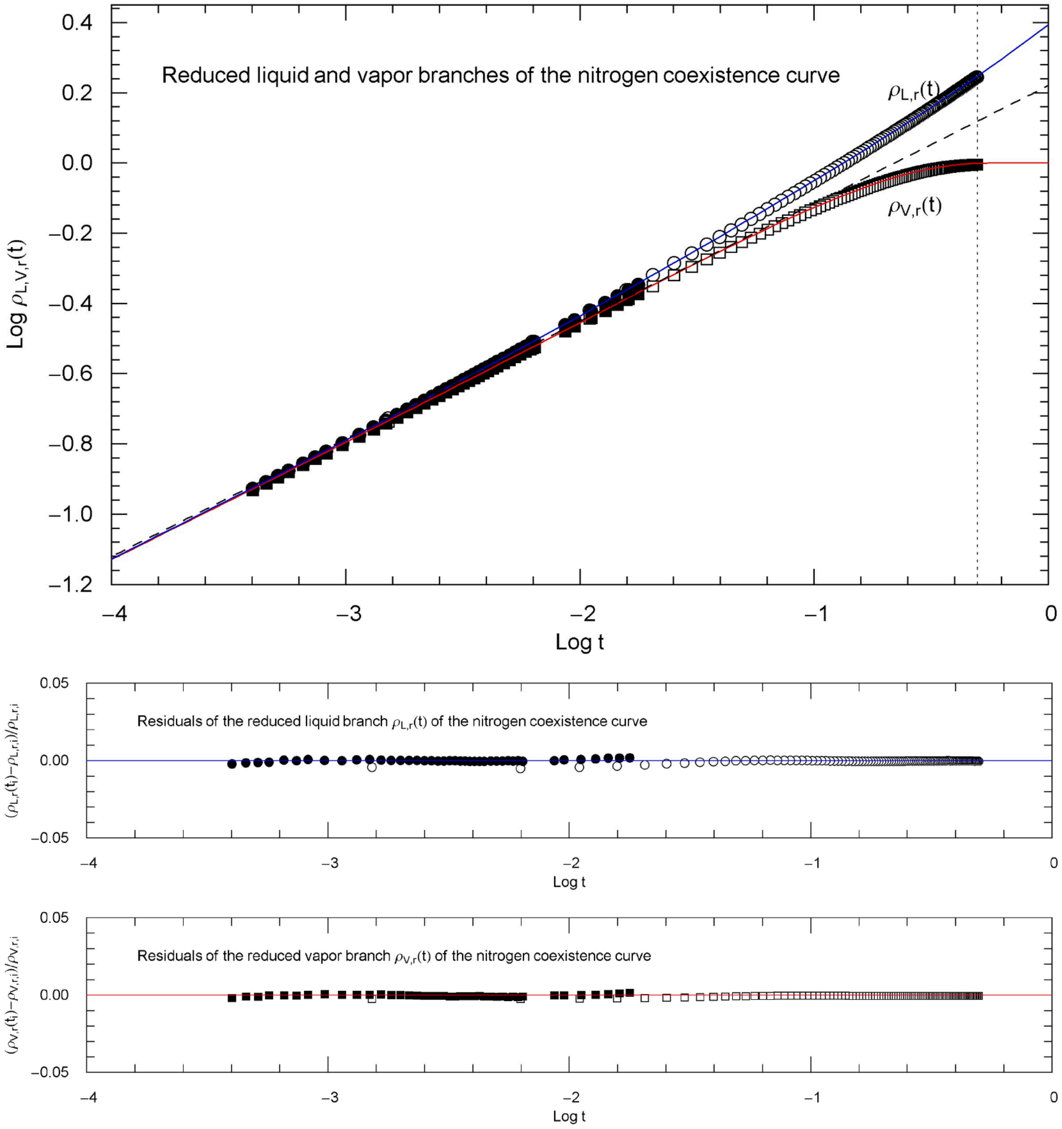

Fig. 2. Reduced liquid and vapor branches of the nitrogen coexistence curve. Data points as in Fig. 1. Depicted are the reduced densities $\rho_{\mathrm{L,r}}(t)$ and $\rho_{\mathrm{V,r}}(t)$ (blue and red solid curves), cf. Sections 2 and 5, obtained from the regressed coexistence curve in Fig. 1. The reduced branches converge to a common asymptote, $\rho_{\mathrm{L,r}}(t) \sim \rho_{\mathrm{V,r}}(t) \sim B_\mathrm{ord} t^\beta$ (black dashed straight line), cf. Section 3.1. The densities do not intersect, $\rho_{\mathrm{L,r}}(t) > \rho_{\mathrm{V,r}}(t)$ throughout the subcritical temperature range. The triple-point temperature is indicated by the vertical dotted line. Residual percentage deviations of the data points from the regressed analytic curves are shown in the lower panels.

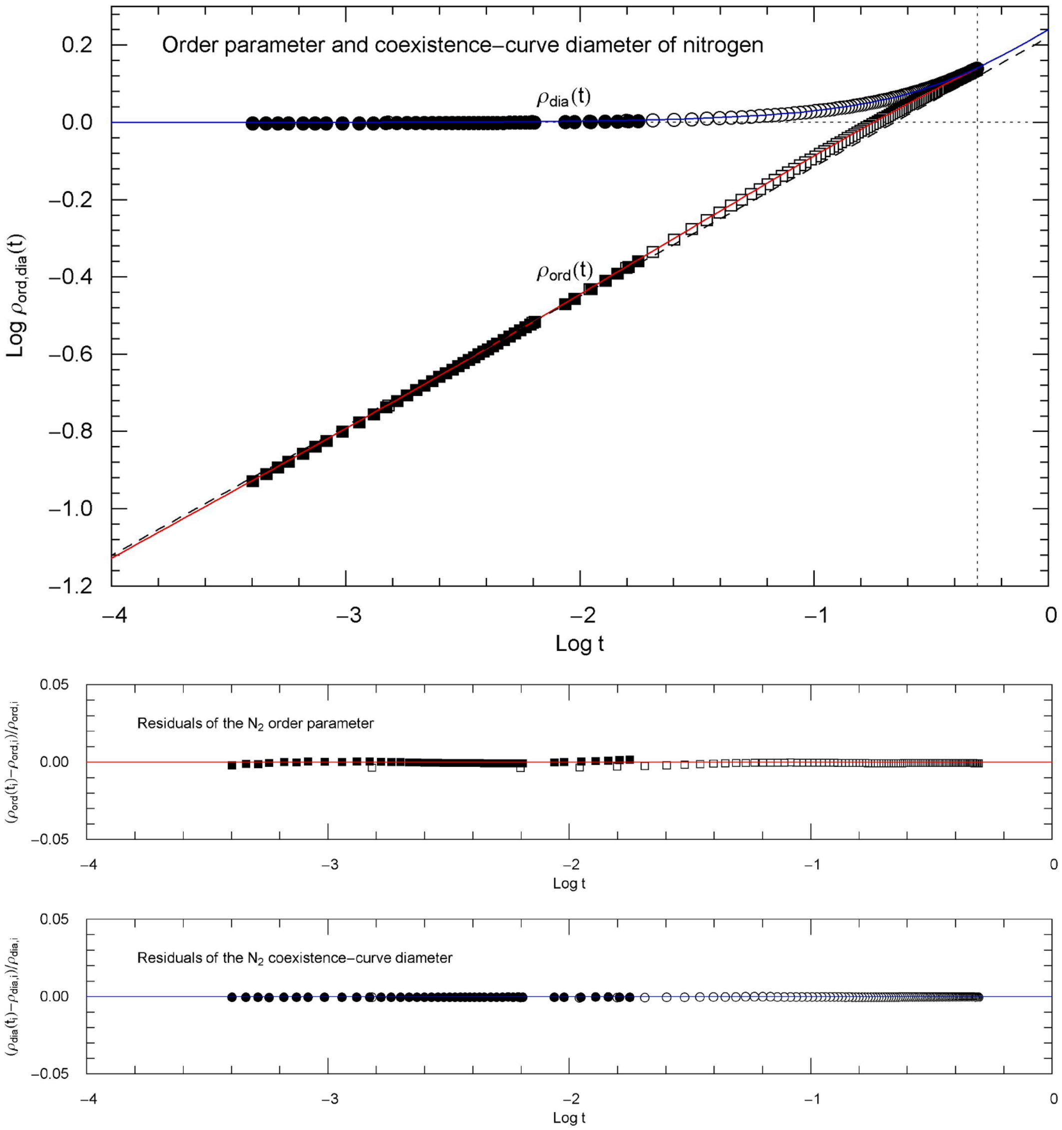

Fig. 3. Order parameter and coexistence-curve diameter of nitrogen. Depicted are the liquid−vapor order parameter $\rho_{\mathrm{ord}}(t)$ (red solid curve) and the coexistence-curve diameter $\rho_{\mathrm{dia}}(t)$ (blue solid curve) assembled from the regressed liquid and vapor branches of the coexistence curve in Fig. 1, cf. Sections 2 and 5. The black dashed straight line is the asymptote of the order parameter, $\rho_{\mathrm{ord}}(t) \sim B_{\mathrm{ord}} t^{\beta}$, cf. Section 3.1. The vertical dotted line indicates the triple-point temperature. Residual plots of the order parameter and diameter are shown in the lower panels.

and liquid branches of the nitrogen coexistence curve and covering a large section of the interval $T_{\mathrm{tr}} \le T \le T_{\mathrm{c}}$ of stable vapor−liquid equilibrium, cf. Refs. [1–3]. The critical point parameters and triple-point temperature of nitrogen are listed in Table 1. The vapor branch has a measurable continuation below the triple point, and it is evident from the Log−Log plot of the data points in Fig. 1 that the vapor curve is exponentially decaying (possibly with a Weibull-type cutoff, cf. Section 3) toward zero temperature. (Power-law decay in double-logarithmic coordinates shows as straight line with negative slope, whereas the tail of the vapor curve in Fig. 1 is substantially curved.) In the opposite limit, close to the critical temperature, the ρ_{c}-normalized densities in Fig. 1 converge to one. Moreover, $\rho_{\mathrm{L}}(t) > 1$ and $\rho_{\mathrm{V}}(t) < 1$ holds over the entire temperature range from the triple point to the critical point, and the liquid branch is monotonically increasing and $\rho_{\mathrm{V}}(t)$ decreasing.

Fig. 2 depicts the data points $(t_i, \rho_{\mathrm{L},i} - 1)_{i=1,\dots,N}$ and $(t_i, 1 - \rho_{\mathrm{V},i})_{i=1,\dots,N}$ of the reduced branches of the nitrogen coexistence curve,

$$\rho_{\mathrm{L,r}}(t) := \rho_{\mathrm{L}} - 1,\ \rho_{\mathrm{V,r}}(t) := 1 - \rho_{\mathrm{V}}, \tag{2.1}$$

also in double-logarithmic coordinates. Since $\rho_{\mathrm{V}}(t\to 1)$ decays exponentially, the reduced vapor density converges to one in this limit. More importantly, the data points in Fig. 2 also suggest that $\rho_{\mathrm{L,r}}(t) > \rho_{\mathrm{V,r}}(t)$ throughout the interval $0 \le t \le 1 - T_{\mathrm{tr}}/T_{\mathrm{c}}$ and that these reduced densities admit, in the critical limit $t\to 0$, a common straight asymptote. We will denote the power law defining this asymptote by $B_{\mathrm{ord}} t^{\beta}$, with positive amplitude B_{ord} and positive exponent β, the latter being the Log−Log slope of the asymptote,

$$\rho_{\mathrm{L,r}}(t) \sim \rho_{\mathrm{V,r}}(t) \sim B_{\mathrm{ord}} t^{\beta}. \tag{2.2}$$

The dimensionless order parameter $\rho_{\mathrm{ord}}(t)$ of the liquid−vapor transition is defined as

$$\rho_{\mathrm{ord}}(t) = \frac{1}{2}(\rho_{\mathrm{L}} - \rho_{\mathrm{V}}) = \frac{1}{2}\left(\rho_{\mathrm{L,r}} + \rho_{\mathrm{V,r}}\right). \tag{2.3}$$

Since the order parameter is the average of the reduced densities, it has the same asymptotic limit, cf., e.g., Refs. [27–30],

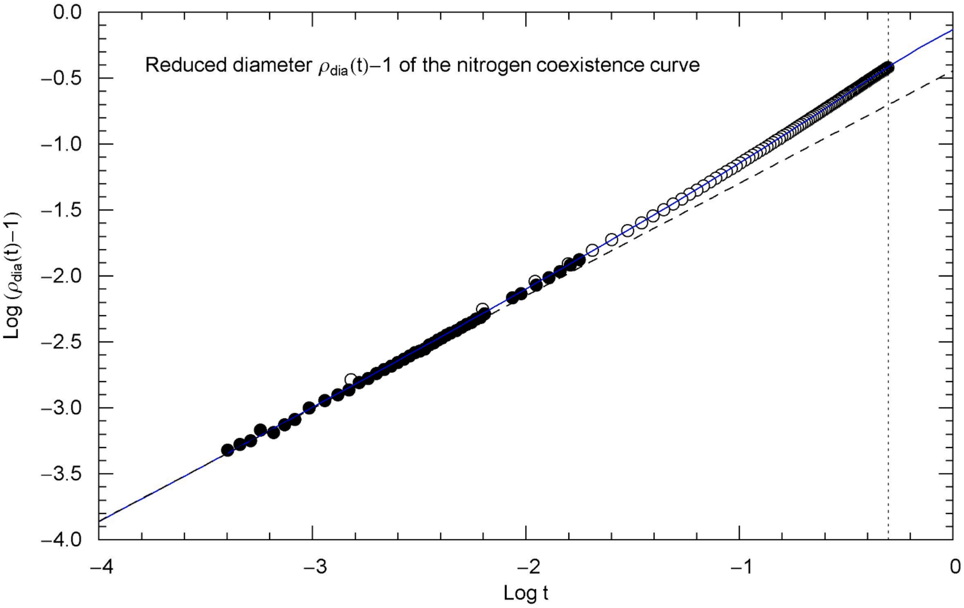

Fig. 4. Reduced coexistence-curve diameter of nitrogen. The blue solid curve depicts the reduced diameter $\rho_{\rm dia,r}(t)$ calculated from the regressed liquid and vapor branches $\rho_{\rm L}(t)$ and $\rho_{\rm V}(t)$ in Fig. 1, cf. Sections 2 and 5. (The unreduced diameter $\rho_{\rm dia}(t)$ is plotted in Fig. 3.) The black dashed straight line is the asymptote of $\rho_{\rm dia,r}(t)$, indicating the power-law scaling of the reduced diameter, cf. after (3.3) and Section 5.

$$\rho_{\rm ord}(t) \sim B_{\rm ord} t^{\beta}. \tag{2.4}$$

The coexistence-curve diameter $\rho_{\rm dia}(t)$ is defined as the average of the liquid and vapor branches of the coexistence curve,

$$\rho_{\rm dia}(t) = \frac{1}{2}(\rho_{\rm L} + \rho_{\rm V}) = 1 + \frac{1}{2}\left(\rho_{\rm L,r} - \rho_{\rm V,r}\right). \tag{2.5}$$

Order parameter and diameter determine the coexistence curve by inversion of (2.3) and (2.5), $\rho_{\rm L} = \rho_{\rm dia} + \rho_{\rm ord}$, $\rho_{\rm V} = \rho_{\rm dia} - \rho_{\rm ord}$. The data points of the order parameter $\rho_{\rm ord}(t)$ and coexistence-curve diameter $\rho_{\rm dia}(t)$ of nitrogen are depicted in Fig. 3, obtained by subtracting or adding the densities of the liquid and vapor branches according to (2.3) and (2.5), which is possible since the experimental liquid and vapor data points $(t_i, \rho_{{\rm L},i})_{i=1,\ldots,N}$ and $(t_i, \rho_{{\rm V},i})_{i=1,\ldots,N}$ in Refs. [1–3] are taken at the same temperatures t_i. The data points of the order parameter are thus $(t_i, \rho_{{\rm ord},i})_{i=1,\ldots,N}$, with $\rho_{{\rm ord},i} = (\rho_{{\rm L},i} - \rho_{{\rm V},i})/2$, and the data points of the diameter depicted in Fig. 3 are $(t_i, \rho_{{\rm dia},i})_{i=1,\ldots,N}$ with $\rho_{{\rm dia},i} = (\rho_{{\rm L},i} + \rho_{{\rm V},i})/2$. If the data points of the liquid and vapor branches are taken at different temperatures, one can use linear interpolation to align them. The least-squares regression in Section 3 will be performed with the liquid and vapor branches $\rho_{\rm L}(t)$ and $\rho_{\rm V}(t)$ of the coexistence curve, where an alignment of the temperatures is not necessary. The curves representing the order parameter and diameter in Fig. 3 are obtained from the regressed liquid and vapor branches $\rho_{\rm L}(t)$, $\rho_{\rm V}(t)$ (see Section 3) by way of (2.3) and (2.5), rather than being directly regressed from the composite data points depicted in Fig. 3.

Finally, the reduced coexistence-curve diameter $\rho_{\rm dia,r}(t)$ is defined as

$$\rho_{\rm dia,r}(t) = \rho_{\rm dia} - 1 = \frac{1}{2}\left(\rho_{\rm L,r} - \rho_{\rm V,r}\right). \tag{2.6}$$

The leading asymptotic order (2.2) of the reduced branches of the coexistence curve drops out in the reduced diameter. The critical power-law scaling of $\rho_{\rm dia,r}(t)$ will be discussed in Sections 3.1 and 5. The data points $(t_i, \rho_{{\rm dia,r},i})_{i=1,\ldots,N}$ of the reduced diameter of nitrogen are depicted in Fig. 4, assembled from the data sets $(t_i, \rho_{{\rm L},i})_{i=1,\ldots,N}$ and $(t_i, \rho_{{\rm V},i})_{i=1,\ldots,N}$ of the liquid and vapor branches of the coexistence curve, $\rho_{{\rm dia,r},i} = (\rho_{{\rm L},i} + \rho_{{\rm V},i})/2 - 1$, cf. (2.5).

Analytic representations of the liquid and vapor branches $\rho_{\rm L}(t)$, $\rho_{\rm V}(t)$ of the coexistence curve, which can be used for molecular fluids as well as liquid metals, will be obtained in Sections 3 and 5 by performing least-squares fits of Weibull-type exponentials and broken power laws to the liquid and vapor saturation data of the respective fluids. It suffices to mention here that the blue and red solid curves in Fig. 1 depict the regressed analytic branches $\rho_{\rm L}(t)$ and $\rho_{\rm V}(t)$ of the nitrogen coexistence curve. All other quantities defined in this section are assembled from the regressed $\rho_{\rm L}(t)$ and $\rho_{\rm V}(t)$ as indicated: The reduced branches $\rho_{\rm L,r}(t)$ and $\rho_{\rm V,r}(t)$, cf. (2.1), are shown in Fig. 2, the nitrogen order parameter (2.3) and diameter (2.5) in Fig. 3, and the reduced diameter (2.6) is depicted in Fig. 4.

3. Liquid and vapor branches of the coexistence curve: critical power-law scaling and Weibull exponential decay

3.1. Analytic closed-form modeling of the coexistence curve

The exponentially decaying vapor branch of the coexistence curve, cf. Section 2 and Fig. 1, is modeled with a Weibull exponential,

$$\rho_{\rm V}(t) = \exp\left(-at^{\beta} - \frac{b_{\rm v} t^{\lambda}}{(1 - t^{\gamma_{\rm v}})^{\eta_{\rm v}}}\right), \tag{3.1}$$

where the reduced temperature $t = 1 - T/T_{\rm c}$ varies in the unit interval $0 \le t \le 1$ between critical and zero temperature. The positive amplitudes a,$b_{\rm v}$ and positive exponents β,λ,$\gamma_{\rm v}$,$\eta_{\rm v}$ are fitting parameters. The power law at^{β} in the exponential is the leading asymptotic order of the reduced density $\rho_{\rm V,r}(t)$ in the critical regime, cf. (2.2) ($a = B_{\rm ord}$). A Weibull cutoff generated by the denominator of the second term in (3.1) is suggested by the double-logarithmic plot of the data points in Fig. 1, so that the vapor density vanishes at $t = 1$; see also Refs. [31,32]. Data points for $\rho_{\rm V}(t)$ are available in the interval $0 \le t \le t_{\rm tr}$, where $t_{\rm tr} = 1 - T_{\rm tr}/T_{\rm c}$ denotes the reduced triple-point temperature, cf. Fig. 1 and Table 1.

The liquid branch of the coexistence curve is defined as a broken power law [33–35] with a Weibull exponential [36] subtracted,

$$\rho_{\rm L}(t) = 2\left(1 + d_l t^{\delta_l}\right)^{\kappa_l} - \exp\left(-at^{\beta} - b_l t^{\lambda}\right). \tag{3.2}$$

Table 2

Fitting parameters of the vapor branch of the N_2, C_2H_4 and SF_6 coexistence curves. The ρ_c-normalized density of the vapor branch reads $\rho_V(t) = \exp(-at^\beta - b_v t^\lambda/(1-t^{\gamma_v})^{\eta_v})$, cf. (3.1). Recorded are the dimensionless parameters of $\rho_V(t)$ and the factor r_c used to recalibrate the critical density in the least-squares functional χ_V^2, cf. Section 3.2. Also listed are the value of χ_V^2 attained at the recorded parameters and the number of data points (# d.p.) defining χ_V^2, as well as the determination coefficient R^2 and the standard error (SE) of the fit.

	a	β	b_v	λ	γ_v	η_v	r_c	χ_V^2	# d.p.	$1-R^2$	SE
N_2	1.6606	0.33533	3.94488	0.854117	1.16852	1.35067	1.00059	6.94×10^{-5}	147	3.10×10^{-7}	1.76×10^{-4}
C_2H_4	1.98999	0.352418	3.68378	0.879336	1.05024	1.37482	0.999943	3.04×10^{-3}	124	1.24×10^{-5}	1.09×10^{-3}
SF_6	1.9006	0.336573	4.76007	0.886211	1.29463	1.59701	0.999363	9.88×10^{-4}	107	1.10×10^{-5}	9.88×10^{-4}

Table 3

Fitting parameters of the liquid branch of the N_2, C_2H_4 and SF_6 coexistence curves. The ρ_c-normalized density of the liquid branch reads $\rho_L(t) = 2(1+d_l t^{\delta_l})^{\kappa_l} - \exp(-at^\beta - b_l t^\lambda)$, cf. (3.2). The amplitude a and exponents β and λ also parametrize the vapor branch, cf. Section 3.1, and are listed in Table 2. The factor r_c for the recalibration of the critical density in the least-squares functional χ_L^2 in (3.9) is also recorded in Table 2. The value of χ_L^2 attained at the recorded parameters, the number of data points (# d.p.) defining χ_L^2, the determination coefficient R^2 and the standard error (SE) of the fit are listed as well.

	b_l	d_l	δ_l	κ_l	χ_L^2	# d.p.	$1-R^2$	SE
N_2	4.66577	4.05119	1.29376	0.341377	1.18×10^{-4}	147	3.77×10^{-7}	3.36×10^{-4}
C_2H_4	4.87461	5.31927	1.36181	0.314869	2.97×10^{-3}	124	1.20×10^{-5}	2.17×10^{-3}
SF_6	6.71908	27.6639	1.76227	0.155748	7.31×10^{-4}	107	7.40×10^{-6}	1.23×10^{-3}

Table 4

Fitting parameters of the vapor branch $\rho_V(t)$ of the N_2, C_2H_4 and SF_6 coexistence curves, assuming 3D Ising critical exponents, cf. Section 5. The caption of Table 2 is applicable, except that the critical exponents β and $\lambda = 1 - \alpha$ are kept fixed at the listed 3D Ising values when minimizing the least-squares functional (3.10).

	a	β	b_v	λ	γ_v	η_v	r_c	χ_V^2	# d.p.	$1-R^2$	SE
N_2	1.57484	0.3264	4.64292	0.8899	1.45495	1.47781	1.00132	3.53×10^{-3}	147	1.31×10^{-5}	1.15×10^{-3}
C_2H_4	1.6597	0.3264	4.72574	0.8899	1.3768	1.45968	1.00132	1.86×10^{-2}	124	9.81×10^{-5}	3.06×10^{-3}
SF_6	1.76075	0.3264	5.33965	0.8899	1.68071	2.1233	0.999688	1.61×10^{-3}	107	1.17×10^{-5}	1.02×10^{-3}

Table 5

Fitting parameters of the liquid branch $\rho_L(t)$ of the N_2, C_2H_4 and SF_6 coexistence curves, assuming 3D Ising critical exponents. The caption of Table 3 is applicable, except that the critical exponents β and $\lambda = 1 - \alpha$ are kept fixed at their 3D Ising values in the regression, cf. Table 4.

	b_l	d_l	δ_l	κ_l	χ_L^2	# d.p.	$1-R^2$	SE
N_2	6.17972	8.51306	1.55262	0.242174	3.98×10^{-4}	147	1.05×10^{-6}	5.64×10^{-4}
C_2H_4	6.9801	12.0215	1.66032	0.224083	4.72×10^{-3}	124	2.15×10^{-5}	2.91×10^{-3}
SF_6	7.65919	46.8217	1.95594	0.133048	1.44×10^{-3}	107	1.16×10^{-5}	1.54×10^{-3}

The amplitudes a, b_l and exponents β, λ in the exponential are positive fitting parameters, as are the exponents δ_l, κ_l and the amplitude d_l in the broken power law suggested by the rectilinear diameter rule for the coexistence-curve diameter, see below. The exponents β, λ and amplitude a are the same as in the vapor branch (3.1), to be determined by a simultaneous least-squares fit of the vapor and liquid branches of the coexistence curve, cf. Section 3.2. Accordingly, the reduced liquid and vapor densities (2.2) admit the same asymptotic scaling, $\rho_{L,r} \sim \rho_{V,r} \sim at^\beta$, assuming that the exponents satisfy $\beta < \lambda < \delta_l$. The fitting parameters of the vapor branch $\rho_V(t)$ of the nitrogen coexistence curve are recorded in Table 2 and the parameters of the liquid branch $\rho_L(t)$ in Table 3.

The exponent β in (3.1) and (3.2) can either be taken as fitting parameter or calculated 3D Ising exponent $\beta = 0.3264$, cf. Ref. [6], assuming the fluid to be in the 3D Ising universality class. Since the available data sets extend into the $|1 - T/T_c| < 10^{-3}$ interval, we will use β as fitting parameter, so that the least-squares regression is entirely based on empirical data without calculated input from renormalization-group theory. (For comparison, we will also perform the regression with β fixed at the quoted 3D Ising value, cf. the end of Section 5 and Tables 4 and 5.) The exponent β is determined as the Log–Log slope of the common asymptote of the reduced liquid and vapor branches of the coexistence curve. For nitrogen, the reduced branches and their asymptote are depicted in Fig. 2, and the regressed scaling exponent β is listed in Table 2.

The order parameter and coexistence-curve diameter are assembled from the liquid and vapor coexistence-curve branches according to (2.3) and (2.5),

$$\rho_{\mathrm{ord,dia}}(t) = (1 + d_l t^{\delta_l})^{\kappa_l} - \frac{1}{2}\exp(-at^\beta)\left[\exp(-b_l t^\lambda) \pm \exp\left(-\frac{b_v t^\lambda}{(1-t^{\gamma_v})^{\eta_v}}\right)\right], \tag{3.3}$$

the upper plus sign in (3.3) referring to the order parameter. By expanding (3.3) in ascending powers subject to $\beta < \lambda < \delta_l$, we find the asymptotic order parameter $\rho_{\mathrm{ord}} \sim at^\beta$ in the critical regime. The leading asymptotic order of the reduced diameter $\rho_{\mathrm{dia,r}}(t)$, cf. (2.6), is $\rho_{\mathrm{dia,r}} \sim (b_l - b_v)t^\lambda/2$, with parameters in Tables 2 and 3. The data sets defining the reduced liquid and vapor branches in Fig. 2 suggest that $\rho_{\mathrm{dia,r}}(t)$ is positive throughout the interval $0 \le t \le t_{\mathrm{tr}}$, which requires $b_l > b_v$. Otherwise, if $b_l < b_v$, the reduced branches of the coexistence curve in Fig. 2 would intersect, cf. (2.6), in contrast to the data sets in Fig. 2, which converge rather than intersect. The first term in (3.3) can be regarded as a generalization of the rectilinear diameter rule $\rho_{\mathrm{dia}}(t) \approx 1 + ct$ for the coexistence-curve diameter, where c is a positive constant, cf., e.g., Refs. [11,12].

Critical scaling theory also makes predictions about the asymptotic scaling of the coexistence-curve diameter, suggesting that the two leading orders of the reduced diameter are the powers $t^{2\beta}$ and $t^{1-\alpha}$, with exponent $\beta = 0.3264$ as above and $\alpha = 0.1101$ (cf. Ref. [6]) being the scaling exponent of the isochoric heat capacity of the 3D Ising model, cf., e.g., Refs. [12–21,37–39]. This scaling can be implemented in the vapor and liquid branches of the coexistence curve by replacing the power law $b_{\rm v}t^{\lambda}$ in (3.1) by the linear combination $b_{\rm v}t^{2\beta} + c_{\rm v}t^{1-\alpha}$ and analogously $b_l t^{\lambda}$ in (3.2) by $b_l t^{2\beta} + c_l t^{1-\alpha}$. The exponents β and α are regarded as calculated constants (e.g., 3D Ising exponents), and the amplitudes b_l, c_l and $b_{\rm v}$, $c_{\rm v}$ are fitting parameters. In addition to the $t^{2\beta}$ and $t^{1-\alpha}$ powers, critical scaling theory and the rectilinear diameter rule also predict a linear term, which is obtained by putting $\delta_l = 1$ in the first term of the liquid density (3.2). In this way, we arrive at

$$\rho_{\rm V}(t) = \exp\left(- at^{\beta} - \frac{b_{\rm v}t^{2\beta} + c_{\rm v}t^{1-\alpha}}{(1 - t^{\gamma_{\rm v}})^{\eta_{\rm v}}}\right), \tag{3.4}$$

$$\rho_{\rm L}(t) = 2(1 + d_l t)^{\kappa_l} - \exp\left[- at^{\beta} - \left(b_l t^{2\beta} + c_l t^{1-\alpha}\right)\right]. \tag{3.5}$$

The order parameter and diameter are assembled as in (3.3), with the indicated substitutions,

$$\rho_{\rm ord,dia}(t) = (1 + d_l t)^{\kappa_l} - \frac{1}{2}\exp\left(- at^{\beta}\right)\left[\exp\left(- b_l t^{2\beta} - c_l t^{1-\alpha}\right) \pm \exp\left(- \frac{b_{\rm v}t^{2\beta} + c_{\rm v}t^{1-\alpha}}{(1 - t^{\gamma_{\rm v}})^{\eta_{\rm v}}}\right)\right]. \tag{3.6}$$

In the least-squares regression, the amplitudes $c_{\rm v}$ and c_l are used as fitting parameters instead of the exponents λ and δ_l, and the exponents β and α are kept fixed. The leading-order scaling of the order parameter is $\rho_{\rm ord} \sim at^{\beta}$ as above, and the leading orders of the reduced diameter are, cf., e.g., Refs. [12,37],

$$\rho_{\rm dia,r} \sim \frac{1}{2}(b_l - b_{\rm v})t^{2\beta} + \frac{1}{2}(c_l - c_{\rm v})t^{1-\alpha} + \kappa_l d_l t. \tag{3.7}$$

The rectilinear diameter approximation is obtained by dropping the exponentials and expanding the first term in (3.6), $\rho_{\rm dia}(t) \approx 1 + \kappa_l d_l t$.

Model calculations in Ref. [12] also indicated that the amplitude $(b_l - b_{\rm v})/2$ of the leading power $t^{2\beta}$ of the reduced diameter (3.7) can be negative. If so, the reduced liquid and vapor branches of the coexistence curve will intersect, which means that $\rho_{\rm V,r}(t)$ will exceed $\rho_{\rm L,r}(t)$ in some temperature interval. Even though intersecting branches are a possibility, there is no evidence for an intersection in the data points depicted in Fig. 2. Moreover, if such an intersection happens, the reduced liquid and vapor branches in Fig. 2 will still have to converge to a common asymptote after the intersection, otherwise the leading power-law amplitudes of $\rho_{\rm V,r}(t)$ and $\rho_{\rm L,r}(t)$ will differ (in contrast to (2.2)), in which case the exponent of the leading order of the reduced diameter $\rho_{\rm dia,r}$ will be β rather than 2β. And even if the amplitude $(b_l - b_{\rm v})/2$ of the leading order is positive, the slope λ (cf. Table 2) of the asymptotic tangent of the reduced diameter in Fig. 4 (dashed straight line) is substantially larger than the calculated exponent 2β, see also Section 5. (This will be further illustrated in Section 4 by Index functions.) The same data sets (depicted in the figures by black symbols) were analyzed in Ref. [3] by means of an ascending series expansion similar to (3.7), and the authors also concluded that a $t^{2\beta}$ power law as leading order of the reduced diameter is not supported by the data.

Therefore, we use a single power law t^{λ} in (3.1) and (3.2), with exponent λ as fitting parameter, instead of the linear combination of $t^{2\beta}$ and $t^{1-\alpha}$ in (3.4)–(3.6) with fixed calculated exponents α and β. In effect, we drop the $t^{2\beta}$ term in (3.4)–(3.6) and let the exponents β and $1-\alpha$ freely float in the regression. The principal aim is to model the coexistence curve over the entire temperature range $0 \le t \le t_{\rm tr}$ between critical point and triple point, based on empirical data, without additional input from critical scaling theory, cf. Section 5. For this reason, we do not attempt to implement correction-to-scaling predictions, e.g., series expansions such as $\rho_{\rm ord} \sim B_{\rm ord}t^{\beta}(1 + B_{\rm ord,1}t^{\Delta} + \cdots)$, where $\Delta = 0.523$ is the leading correction-to-scaling exponent of the 3D Ising model [6], which can only be used in the vicinity of the critical temperature, typically in the interval $|1 - T/T_{\rm c}| < 0.1$ or an even smaller one, cf. Refs. [27–30].

3.2. *Least-squares regression of the coexistence curve*

The least-squares functional used for the fit of the vapor branch (3.1) of the coexistence curve reads

$$\chi^2_{\rm V}(a,\beta,\lambda,b_{\rm v},\gamma_{\rm v},\eta_{\rm v},r_{\rm c}) = \sum_{i=1}^{N}\frac{\left(\rho_{\rm V}(t_i) - r_{\rm c}\rho_{{\rm V},i}\right)^2}{r_{\rm c}^2\rho_{{\rm V},i}^2} + \sum_{i=1}^{N}\frac{\left(\rho_{\rm V}(t_i) - r_{\rm c}\rho_{{\rm V},i}\right)^2}{\left(1 - r_{\rm c}\rho_{{\rm V},i}\right)^2}, \tag{3.8}$$

where $(t_i, \rho_{{\rm V},i})_{i=1,\dots,N}$ are data points and $\rho_{\rm V}(t; a,\beta,\lambda,b_{\rm v},\gamma_{\rm v},\eta_{\rm v})$ is the Weibull density (3.1). The experimental densities $\rho_{{\rm V},i}$ are normalized with the critical density $\rho_{\rm c}$, so that $\rho_{{\rm V},i}$ is dimensionless. The data points of Ref. [3], depicted as black symbols in the figures, cover a temperature interval close to $T_{\rm c}$. The data points indicated by the open symbols are spread over a subcritical temperature range further away from $T_{\rm c}$, extending to the triple point; these data and also the critical-point parameters quoted in Table 1 are taken from Refs. [1,2]. The parameter $r_{\rm c}$ in (3.8) is a fitting parameter used to renormalize the experimental data points (more precisely, to renormalize the critical density $\rho_{\rm c} \to \rho_{\rm c}/r_{\rm c}$ used for the normalization of the experimental densities $\rho_{{\rm V},i}$). The regressed $r_{\rm c}$ is always very close to one, cf. Table 2, and only has a noticeable effect on the data points of the reduced diameter, cf. Fig. 4. (The data points $(t_i, \rho_{{\rm V},i})_{i=1,\dots,N}$ depicted in the figures are normalized with the rescaled critical density $\rho_{\rm c}/r_{\rm c}$.) An analogous renormalization of the critical density was used in Ref. [3], where the normalized diameter with constant limit $\rho_{\rm dia}(t \to 0) \sim 1$ in (2.5) was regressed in the vicinity of the critical temperature based on the series expansion $\rho_{\rm dia} = a + bt^{2\beta} + ct^{1-\alpha} + dt + \cdots$, cf. (3.7), with coefficient a treated as fitting parameter slightly deviating from 1, which amounts to an adjustment of the critical density used for the normalization of the data points.

The weight factors $r_{\rm c}^2\rho_{{\rm V},i}^2$ of the first series in (3.8) go to zero for $t \to 1$ due to the exponential decay of the vapor branch in this limit, and they converge to one close to the critical temperature (cf. Fig. 1), in which case the ratios do not significantly contribute to the χ^2 functional. The reverse holds true for the weights $(1 - r_{\rm c}\rho_{{\rm V},i})^2$ in the second series, so that both the exponential decay as well as the approach to the critical point are adequately presented by the χ^2 functional. In effect, the first series in (3.8) is the χ^2 functional for the vapor branch $\rho_{\rm V}(t)$, and the second series the χ^2 functional for the reduced vapor branch $\rho_{\rm V,r}(t) = 1 - \rho_{\rm V}(t)$.

Analogously, the regression of the liquid branch of the coexistence curve is based on the least-squares functional

$$\chi^2_{\rm L}(a,\beta,\lambda,b_l,d_l,\delta_l,\kappa_l,r_{\rm c}) = \sum_{i=1}^{N}\frac{\left(\rho_{\rm L}(t_i) - r_{\rm c}\rho_{{\rm L},i}\right)^2}{r_{\rm c}^2\rho_{{\rm L},i}^2} + \sum_{i=1}^{N}\frac{\left(\rho_{\rm L}(t_i) - r_{\rm c}\rho_{{\rm L},i}\right)^2}{\left(r_{\rm c}\rho_{{\rm L},i} - 1\right)^2}, \tag{3.9}$$

where $(t_i, \rho_{{\rm L},i})_{i=1,\dots,N}$ are the data points of the liquid branch of the coexistence curve and $\rho_{\rm L}(t; a,\beta,\lambda,b_l,d_l,\delta_l,\kappa_l)$ in (3.9) is the analytic representation (3.2) of the liquid branch.

Since the parameters $a,\beta,\lambda,r_{\rm c}$ appear in both functionals (3.8) and (3.9), we perform a simultaneous fit of the vapor and liquid branches by adding the two functionals,

$$\chi^2_{\rm V+L} = \chi^2_{\rm V}(a,\beta,\lambda,b_{\rm v},\gamma_{\rm v},\eta_{\rm v},r_{\rm c}) + \chi^2_{\rm L}(a,\beta,\lambda,b_l,d_l,\delta_l,\kappa_l,r_{\rm c}). \tag{3.10}$$

The regressed parameters of the branches $\rho_{\rm V}(t)$, $\rho_{\rm L}(t)$ of the coexistence curve, cf. (3.1), (3.2), are listed in Tables 2 and 3 for the respective

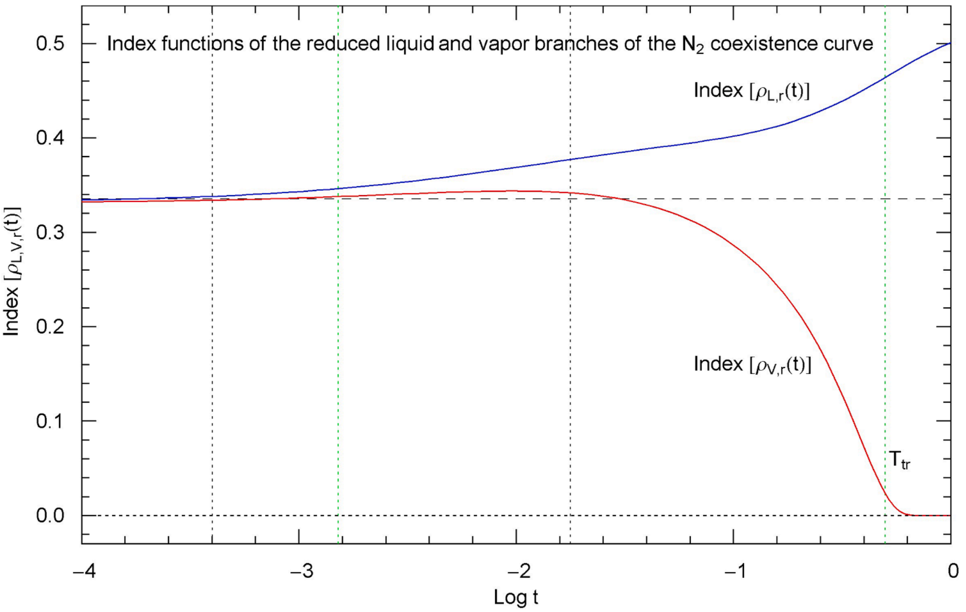

Fig. 5. Index functions (effective exponents) of the reduced liquid and vapor densities of the nitrogen coexistence curve. The blue and red solid curves Index$[\rho_{L,r}(t)]$ and Index$[\rho_{V,r}(t)]$ show the temperature evolution of the Log−Log slope of the reduced coexistence-curve branches in Fig. 2, cf. Sections 4 and 5. The vertical black dotted lines indicate the temperature interval covered by data points of Ref. [3] (black filled symbols in Fig. 2) and the vertical green dotted lines the interval covered by data points from Refs. [1,2] (open symbols in Fig. 2). The horizontal dashed line is the common asymptote of the Index curves, representing the constant Index function (scaling exponent) of the asymptotic power law $B_{\mathrm{ord}}t^{\beta}$ (dashed straight line in Fig. 2).

fluids, obtained by minimizing $\chi^2_{\mathrm{V+L}}$ in (3.10). A suitable Mathematica® [40] routine for the minimization of the nonlinear $\chi^2_{\mathrm{V+L}}$ functional is FindMinimum[{chisquared[...],positivity constraints},{initial values}, MaxIterations→nmax].

The standard error (SE) and the coefficient of determination R^2 of the least-squares fits of $\rho_{\mathrm{V}}(t)$ and $\rho_{\mathrm{L}}(t)$ are also listed in Tables 2 and 3. The standard error is calculated as $\mathrm{SE} = \left(\sum_{i=1}^{N}(\rho(t_i) - r_c\rho_i)^2/N\right)^{1/2}$ (where we have dropped the V or L subscript on the densities, cf. (3.8) and (3.9)). The determination coefficient is assembled as $R^2 = 1 - \sum_{i=1}^{N}(\rho(t_i) - r_c\rho_i)^2/(N\sigma_s^2)$, cf. Ref. [41], with sample variance $\sigma_s^2 = \sum_{i=1}^{N}(r_c\rho_i - \bar{\rho})^2/N$ and mean $\bar{\rho} = \sum_{i=1}^{N} r_c\rho_i/N$.

To obtain error estimates of the regressed parameters, it suffices to calculate the covariance matrix separately from the χ^2 functional of each density. We sketch this at hand of the vapor density $\rho_{\mathrm{V}}(t)$ in (3.1), which depends on six parameters $a, b_{\mathrm{v}}, \beta, \lambda, \gamma_{\mathrm{v}}, \eta_{\mathrm{v}}$. It is convenient to rename these parameters, in the indicated order, as c_k, $k = 1, \dots, 6$, writing $\rho_{\mathrm{V}}(t; (c_k)_{k=1,\dots,6})$ for density (3.1). The covariance matrix is calculated from the functional

$$\chi^2\left((c_k)_{k=1,\dots,6}\right) = \sum_{i=1}^{N} \frac{\left[\rho_{\mathrm{V}}\left(t_i; (c_k)_{k=1,\dots,6}\right) - r_c\rho_{\mathrm{V},i}\right]^2}{\sigma_i^2}, \tag{3.11}$$

where the σ_i^2 are the variances of the data points $(t_i, \rho_{\mathrm{V},i})_{i=1,\dots,N}$, cf. (3.8). The scale factor r_c of the critical density ρ_c is kept constant at the regressed value. The error margin for the synthetic saturation data of nitrogen (depicted by open symbols in the figures) is indicated in Ref. [2] as 0.02 %. An error bound for the SF$_6$ data of Ref. [3] in the near-critical region (black filled symbols) is quoted in Ref. [42] as 0.05 %. Accordingly we use, for lack of individual error bounds on the data points, the conservative estimate $\sigma_i = 5\times10^{-4} r_c\rho_{\mathrm{V},i}$ for the standard deviations. Substituting this into (3.11), the first series in (3.8) is recovered, up to a constant factor.

The Hessian matrix of $\chi^2/2$, cf. (3.11), is evaluated at the regressed parameters $(c_k)_{k=1,\dots,6} = (a, b_{\mathrm{v}}, \beta, \lambda, \gamma_{\mathrm{v}}, \eta_{\mathrm{v}})$ recorded in Table 1,

$$\mathrm{hes}_{ij} := \frac{1}{2}\frac{\partial^2}{\partial c_i \partial c_j}\chi^2\left((c_k)_{k=1,\dots,6}\right), \tag{3.12}$$

$i, j = 1, \dots, 6$. The factor of 1/2 stems from the Taylor expansion of χ^2 at the regressed parameters. Neglecting terms depending on second-order c_k derivatives of $\rho_{\mathrm{V}}(t; (c_k)_{k=1,\dots,6})$, the Hessian is approximated as, cf., e.g., Ref. [43],

$$\mathrm{hes}_{ij} = \sum_{l=1}^{N} \frac{1}{\sigma_l^2}\frac{\partial\rho_{\mathrm{V}}(t_l)}{\partial c_i}\frac{\partial\rho_{\mathrm{V}}(t_l)}{\partial c_j}, \tag{3.13}$$

which is positive definite, being the sum of positive definite matrices. The derivatives needed in (3.13) can readily be obtained analytically with Mathematica® [40]. The covariance matrix is the inverse of the Hessian, $\mathrm{cov}_{ij} = (\mathrm{hes}^{-1})_{ij}$, and the variances of the regressed parameters are the diagonal elements thereof. Error bounds for the exponents β and λ, cf. Section 3.1, will be quoted at the end of Section 5.

4. Index functions (effective exponents) of coexistence curves

The Index function of a density $\rho(t)$ is defined as, cf., e.g., Refs. [22, 23,44]

$$\mathrm{Index}[\rho(t)] := t\frac{\rho'(t)}{\rho(t)} = \frac{\mathrm{dlog}\rho(t)}{\mathrm{dlog}t}, \tag{4.1}$$

which gives the Log−Log slope of the $\rho(t)$ curve, i.e. the slope in double-logarithmic coordinates used in the figures. (In Log−Log coordinates, a tangent line of $\rho(t)$ represents a simple power law with the slope parameter as exponent.) Positivity of $\rho(t)$ and t is not required in the first definition in (4.1).

In critical scaling theory, the Index function was introduced as temperature-dependent effective exponent in Ref. [22]. If $\rho(t)$ converges asymptotically to a power law, its effective exponent Index$[\rho(t)]$ converges to the power-law exponent. In economics, the Index function (4.1) is known as elasticity of the respective density, cf., e.g., Refs. [45, 46].

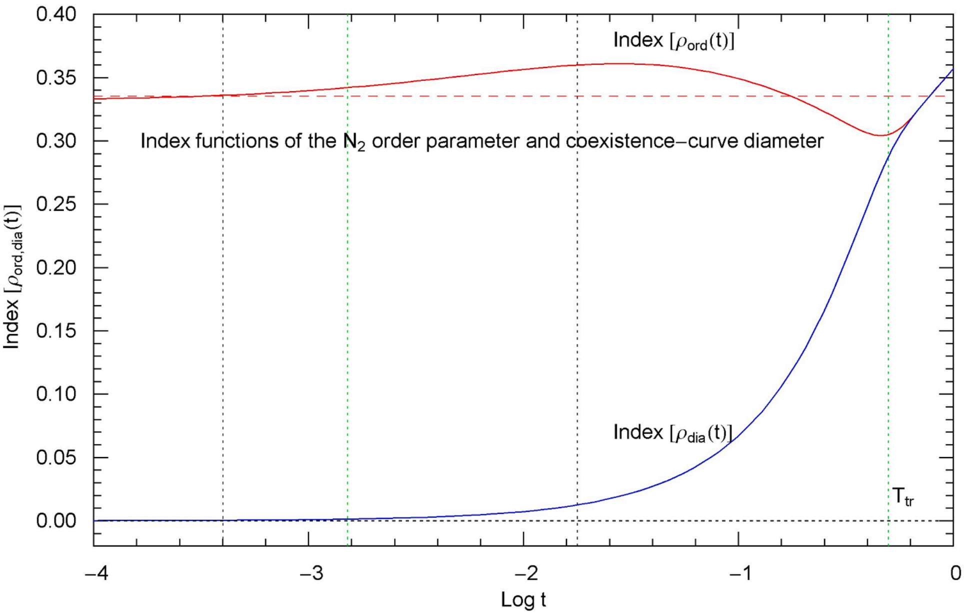

Fig. 6. Index functions (effective exponents) of the order parameter and coexistence-curve diameter of nitrogen. The red and blue solid curves show the slope evolution Index$[\rho_{\mathrm{ord}}(t)]$ and Index$[\rho_{\mathrm{dia}}(t)]$ of the order parameter and diameter in Fig. 3, cf. Sections 4 and 5. The vertical black dotted lines indicate the temperature interval covered by data points of Ref. [3] (black filled symbols in Fig. 3) and the vertical green dotted lines the interval covered by data points from Refs. [1,2] (open symbols in Fig. 3). The horizontal red dashed line, asymptotically tangent to the Index$[\rho_{\mathrm{ord}}(t)]$ curve, depicts the constant Index function Index$[B_{\mathrm{ord}}t^\beta] = \beta$ of the asymptotic order parameter $B_{\mathrm{ord}}t^\beta$ (black dashed straight line in Fig. 3).

The Index of a simple power law at^α is independent of the amplitude and coincides with the power-law exponent, Index$[at^\alpha] = \alpha$. For the Index of a broken power law $(c+dt^\delta)^\kappa$, cf. (3.2), we find

$$\mathrm{Index}[(c+dt^\delta)^\kappa] = \kappa\delta\frac{dt^\delta}{c+dt^\delta}. \tag{4.2}$$

The Index functions of the Weibull exponentials $\exp(-bt^\lambda)$ and $\exp(-bt^\lambda/(1-t^\gamma)^\eta)$ in (3.1) read $\mathrm{Index}[\exp(-bt^\lambda)] = -\lambda bt^\lambda$ and

$$\mathrm{Index}\left[\exp\left(\frac{-bt^\lambda}{(1-t^\gamma)^\eta}\right)\right] = \frac{-bt^\lambda}{(1-t^\gamma)^\eta}\left(\lambda+\gamma\eta\frac{t^\gamma}{1-t^\gamma}\right). \tag{4.3}$$

To calculate the Index of the vapor and liquid branches $\rho_{\mathrm{V}}(t)$, $\rho_{\mathrm{L}}(t)$ of the coexistence curve in (3.1) and (3.2), one can use (4.2), (4.3) and the multiplication and addition rules

$$\mathrm{Index}\left[\rho_1\rho_2^{\pm1}\right] = \mathrm{Index}[\rho_1] \pm \mathrm{Index}[\rho_2], \tag{4.4}$$

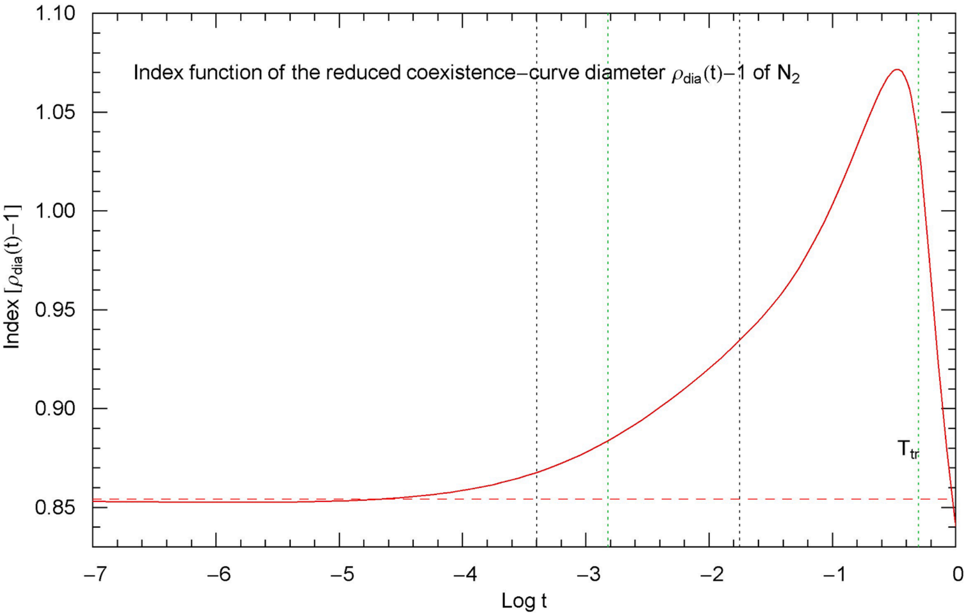

Fig. 7. Index function (effective exponent) of the reduced coexistence-curve diameter of nitrogen. Depicted is the Index function Index$[\rho_{\mathrm{dia,r}}(t)]$ (red solid curve), cf. Sections 4 and 5, of the reduced diameter in Fig. 4, representing the temperature evolution of the Log−Log slope of $\rho_{\mathrm{dia,r}}(t)$. The vertical black dotted lines indicate the temperature interval covered by data points of Ref. [3] (black filled symbols in Fig. 4) and the vertical green dotted lines the interval covered by data points from Refs. [1,2] (open symbols in Fig. 4). The horizontal red dashed line is the asymptote of the Index$[\rho_{\mathrm{dia,r}}(t)]$ curve, depicting the constant Index function (scaling exponent) of the asymptotic power-law limit of $\rho_{\mathrm{dia,r}}(t)$ (black dashed straight line in Fig. 4), cf. after (3.3) and Section 5.

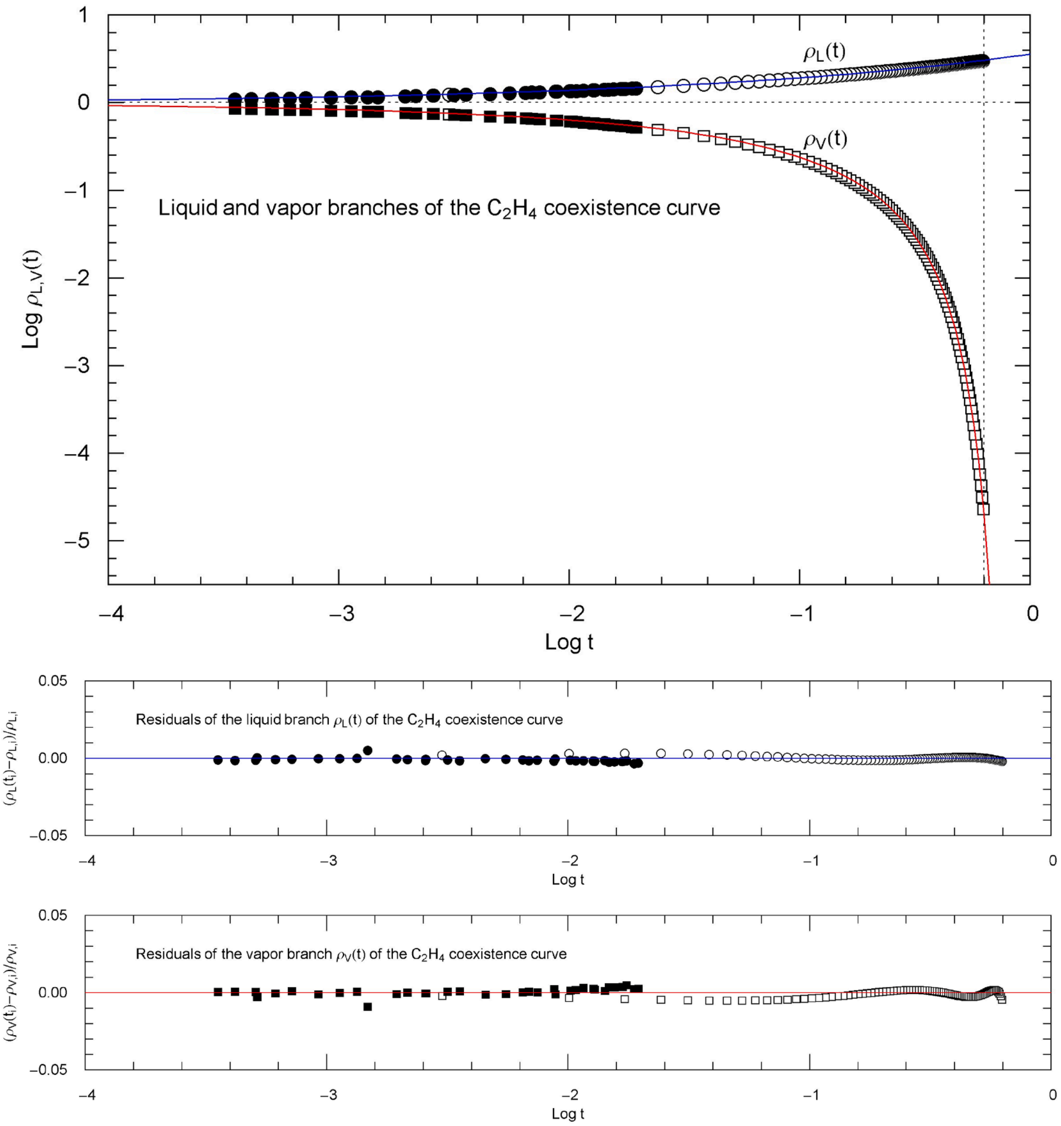

Fig. 8. Coexistence curve of ethylene. Depicted are the liquid and vapor branches $\rho_L(t)$ and $\rho_V(t)$ of the coexistence curve, cf. Sections 2 and 5. The data sets are from Ref. [3] (filled symbols) and Refs. [1,2] (open symbols). The vertical dotted line indicates the ethylene triple-point temperature, cf. Table 1. The blue and red solid curves show the regressed branches $\rho_L(t)$ and $\rho_V(t)$ in (3.1) and (3.2), with fitting parameters in Tables 2 and 3. Residual plots of the regressed branches are shown in the lower panels.

$$\mathrm{Index}[\rho_1 \pm \rho_2] = \frac{\rho_1 \mathrm{Index}[\rho_1] \pm \rho_2 \mathrm{Index}[\rho_2]}{\rho_1 \pm \rho_2}, \tag{4.5}$$

where $\rho_1(t)$ and $\rho_2(t)$ denote arbitrary densities (not necessarily positive). We will not state the explicit equations for the Index functions $\mathrm{Index}[\rho_V(t)]$ and $\mathrm{Index}[\rho_L(t)]$ here, since they are lengthy and can also be obtained by using the primary definition (4.1) of the Index and computer algebra software [40].

The Index of a reduced density reads $\mathrm{Index}[\pm(\rho-1)] = \mathrm{Index}[\rho]\rho/(\rho-1)$, cf. (2.1). The Index functions of the reduced liquid and vapor branches $\rho_{L,r}(t) = \rho_L - 1$, $\rho_{V,r}(t) = 1 - \rho_V$ of the coexistence curve of nitrogen (cf. (2.1), (3.1), (3.2) and Tables 2 and 3) are depicted in Fig. 5 and show the evolution of the Log−Log slope (effective exponent) of the $\rho_{L,r}(t)$ and $\rho_{V,r}(t)$ curves in Fig. 2. Also indicated in Fig. 5 is the constant Index function $\mathrm{Index}[B_{\mathrm{ord}}t^{\beta}] = \beta$ (horizontal black dashed line asymptotically tangential to the Index curves) of the power law $B_{\mathrm{ord}}t^{\beta}$ depicted in Fig. 2 as common asymptote of the reduced densities $\rho_{L,r}(t)$ and $\rho_{V,r}(t)$.

The Index functions of the order parameter, $\mathrm{Index}[\rho_{\mathrm{ord}}(t)] = \mathrm{Index}[\rho_L - \rho_V]$, cf. (2.3), and coexistence-curve diameter, $\mathrm{Index}[\rho_{\mathrm{dia}}(t)] = \mathrm{Index}[\rho_L + \rho_V]$, cf. (2.5), are calculated from the regressed coexistence-curve branches ρ_L, ρ_V in (3.1), (3.2) and Tables 2 and 3, using the addition rule (4.5). These Index functions are plotted in Fig. 6, depicting the Log−Log slope (effective exponent) of the nitrogen order parameter and diameter in Fig. 3. The constant Index function of the asymptotic limit $B_{\mathrm{ord}}t^{\beta}$ of the order parameter (black dashed straight line in Fig. 3) is also indicated in Fig. 6 as horizontal red dashed line asymptotically tangent to the Index curve $\mathrm{Index}[\rho_{\mathrm{ord}}(t)]$. The zero Index function of the constant asymptotic limit of the diameter curve $\rho_{\mathrm{dia}}(t)$ in Fig. 3 is shown as black dotted horizontal line in Fig. 6.

Fig. 7 depicts the Index curve $\mathrm{Index}[\rho_{\mathrm{dia}} - 1] = \mathrm{Index}[\rho_{\mathrm{dia}}]\rho_{\mathrm{dia}}/(\rho_{\mathrm{dia}} - 1)$ of the reduced coexistence-curve diameter $\rho_{\mathrm{dia,r}}(t) = \rho_{\mathrm{dia}} - 1$ of nitrogen, cf. (2.6), plotted in Log−Log coordinates in Fig. 4. As pointed out after (3.3), the asymptotic limit of the reduced diameter is the power law $\rho_{\mathrm{dia,r}} \sim (b_l - b_v)t^{\lambda}/2$ (with parameters listed in Tables 2 and 3 for nitrogen), depicted as black dashed straight line in Fig. 4, asymptotically tangent to the $\rho_{\mathrm{dia,r}}(t)$ curve. The constant Index function $\mathrm{Index}[(b_l - b_v)t^{\lambda}/2] = \lambda$ of this power law is shown in Fig. 7 as asymptote (red dashed horizontal line) to the Index curve $\mathrm{Index}[\rho_{\mathrm{dia,r}}(t)]$

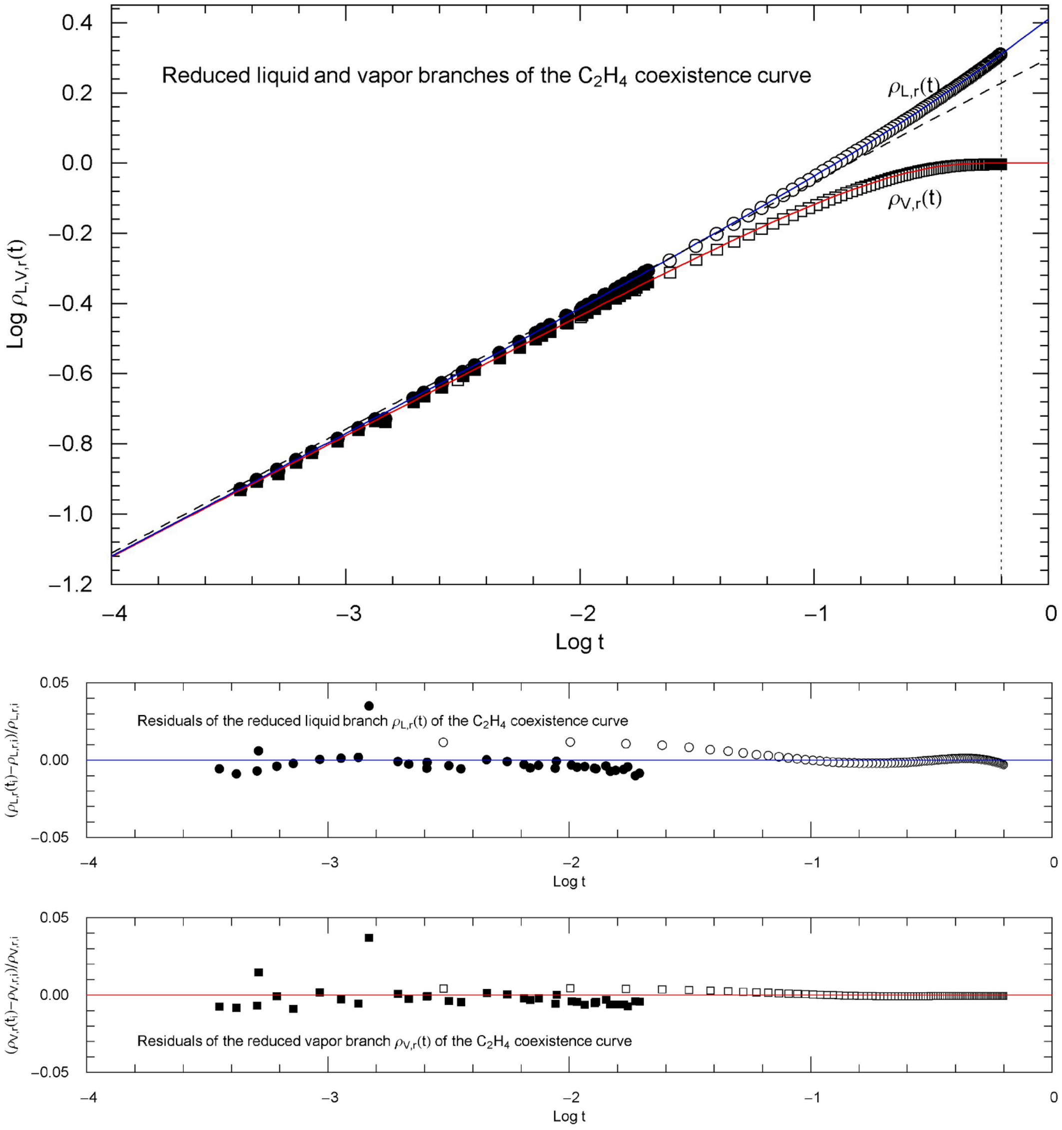

Fig. 9. Reduced liquid and vapor branches of the C_2H_4 coexistence curve. Data points as in Fig. 8. Depicted are the reduced densities $\rho_{\mathrm{L,r}}(t)$ and $\rho_{\mathrm{V,r}}(t)$ (blue and red solid curves), cf. Sections 2 and 5, obtained from the regressed coexistence curve in Fig. 8. The reduced branches converge to a common asymptote, $\rho_{\mathrm{L,r}}(t) \sim \rho_{\mathrm{V,r}}(t) \sim B_{\mathrm{ord}} t^{\beta}$ (black dashed straight line), cf. Sections 2 and 3.1. Residual percentage deviations of the regressed curves are shown in the lower panels.

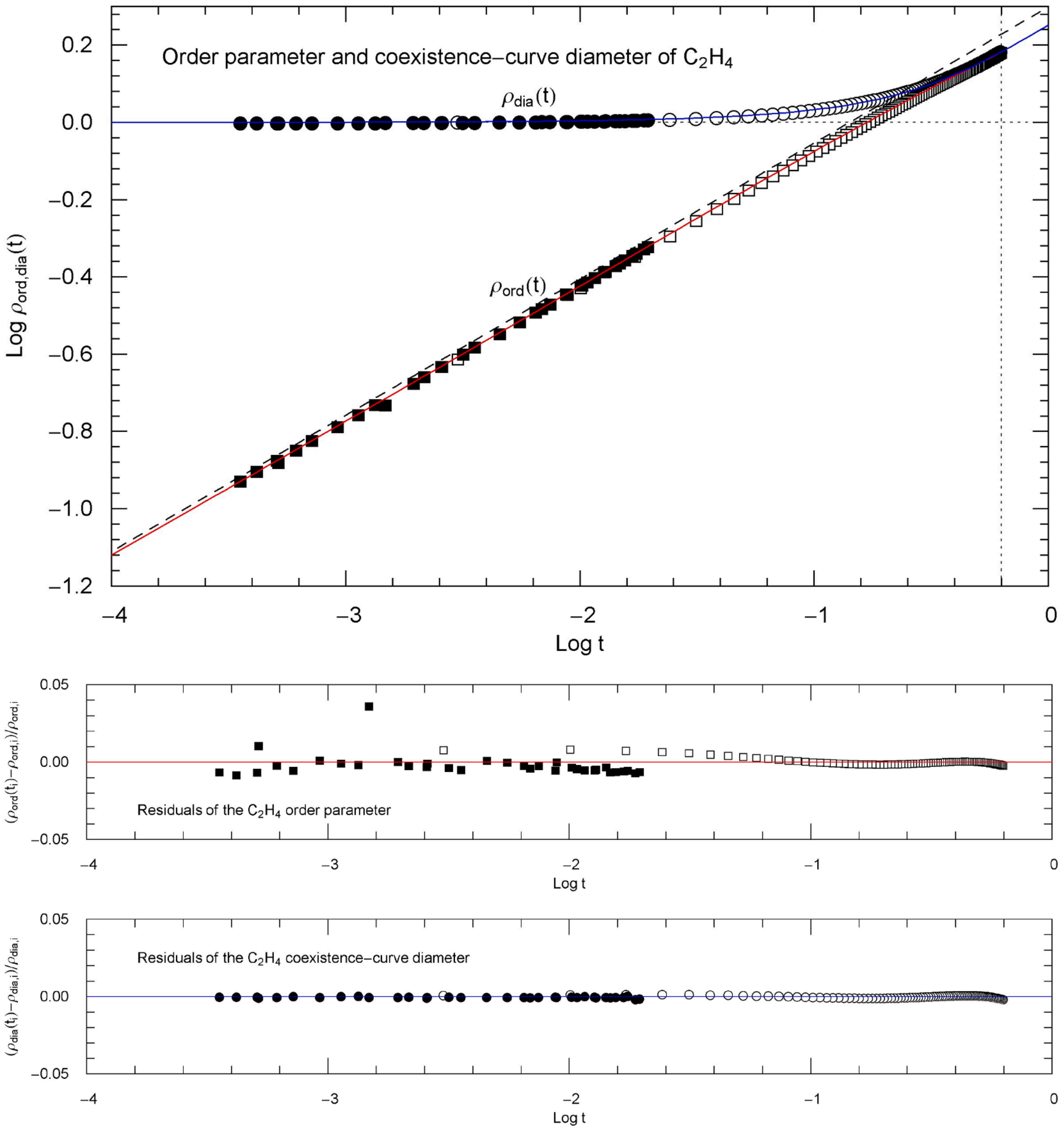

Fig. 10. Order parameter and coexistence-curve diameter of ethylene. Depicted are the liquid–vapor order parameter $\rho_{\text{ord}}(t)$ (red solid curve) and the coexistence-curve diameter $\rho_{\text{dia}}(t)$ (blue solid curve) assembled from the regressed liquid and vapor branches of the coexistence curve in Fig. 8, cf. Sections 2 and 5. The black dashed straight line is the asymptote of the order parameter, representing the critical power-law scaling $\rho_{\text{ord}}(t) \sim B_{\text{ord}} t^{\beta}$, cf. Section 3.1. The vertical dotted line indicates the triple-point temperature, cf. Table 1. Residual plots of the order parameter and diameter are shown in the lower panels.

of the reduced diameter. The Index functions in Figs. 5–7 are plotted in Lin-Log (linear ordinate) representation.

5. Results and discussion: coexistence curves of nitrogen, ethylene, and sulfur hexafluoride

Figs. 1–7 depict the coexistence curve, order parameter and coexistence-curve diameter of nitrogen (N_2) including the Index curves, cf. Figs. 5–7, representing the Log–Log slope (effective exponent) of these temperature-dependent variables. Figs. 8–14 show the same quantities for ethylene (C_2H_4) and Figs. 15–21 for sulfur-hexafluoride (SF_6). The critical parameters and triple-point temperature of N_2, C_2H_4 and SF_6 are listed in Table 1 and the regressed parameters of the depicted coexistence curves are recorded in Tables 2 and 3.

Figs. 1, 8 and 15 show the liquid and vapor branches $\rho_L(t)$, $\rho_V(t)$, cf. (3.1) and (3.2), of the coexistence curve of N_2, C_2H_4 and SF_6, respectively, in double-logarithmic representation, parametrized with reduced temperature $t = 1 - T/T_c$. The data sets close to the critical temperature (black symbols in the figures) are taken from Ref. [3], and the data points depicted as open symbols are synthetic data from Refs. [1,2] covering temperatures down to the triple point. The regressed coexistence-curve branches $\rho_L(t)$, $\rho_V(t)$ are elementary analytic functions, cf. (3.1) and (3.2), and do not involve truncated perturbative series expansions. Residuals of the least-squares fits of $\rho_L(t)$ and $\rho_V(t)$ are depicted in the lower panels of Figs. 1, 8, 15, indicating deviations of less than one percent from the data sets. The least-squares functionals used for the regression of $\rho_L(t)$ and $\rho_V(t)$ are stated in (3.8) and (3.9).

Figs. 2, 9 and 16 show the reduced branches of the N_2, C_2H_4 and SF_6 coexistence curves, that is $\rho_{L,r}(t) = \rho_L(t) - 1$ and $\rho_{V,r}(t) = 1 - \rho_V(t)$, cf. Section 2, also in double-logarithmic representation, which exhibit the asymptotic power-law scaling $\rho_{L,r}(t) \sim \rho_{V,r}(t) \sim B_{\text{ord}} t^{\beta}$, cf. (2.2) and after (3.2). The asymptote $B_{\text{ord}} t^{\beta}$ is depicted in the figures as dashed straight line with Log–Log slope β, cf. Table 2, asymptotically tangential to $\rho_{L,r}(t)$ and $\rho_{V,r}(t)$. (Simple power laws appear as straight lines in Log–Log plots, cf. Section 4.) $\rho_V(t)$ and $\rho_L(t)$ are the coexistence-curve branches in (3.1) and (3.2), with parameters in Tables 2 and 3. The depicted data points are the same as in Figs. 1,8,15, apart from the reduced representation, cf. Section 2, and their residuals with respect to

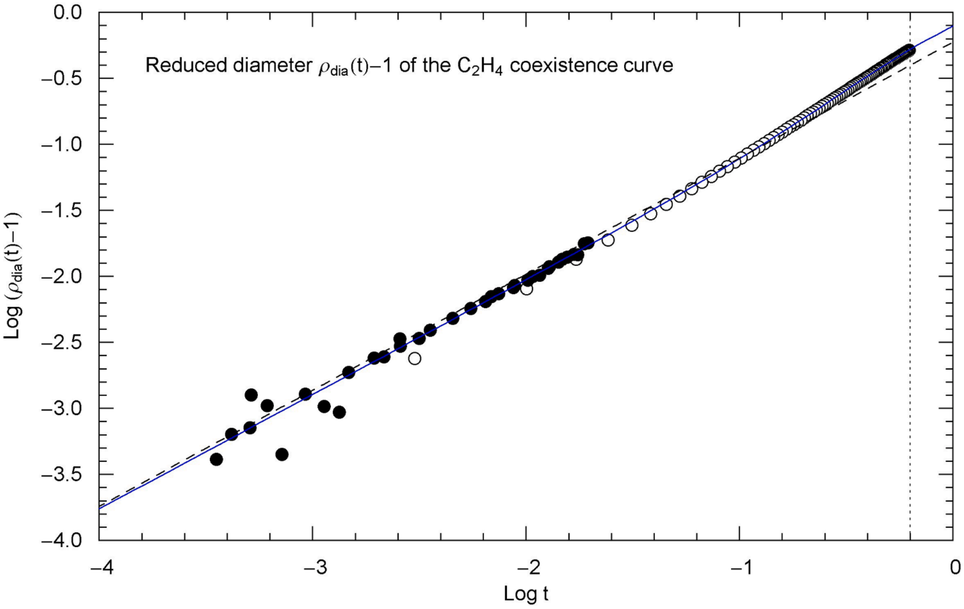

Fig. 11. Reduced coexistence-curve diameter of ethylene. The blue solid curve depicts the reduced diameter $\rho_{\mathrm{dia,r}}(t)$ calculated from the regressed liquid and vapor branches $\rho_{\mathrm{L}}(t)$ and $\rho_{\mathrm{V}}(t)$ in Fig. 8, cf. Sections 2 and 5. The black dashed straight line is the asymptote of $\rho_{\mathrm{dia,r}}(t)$, depicting the power-law scaling of the reduced diameter, cf. after (3.3) and Section 5. The vertical dotted line indicates the triple-point temperature, cf. Table 1.

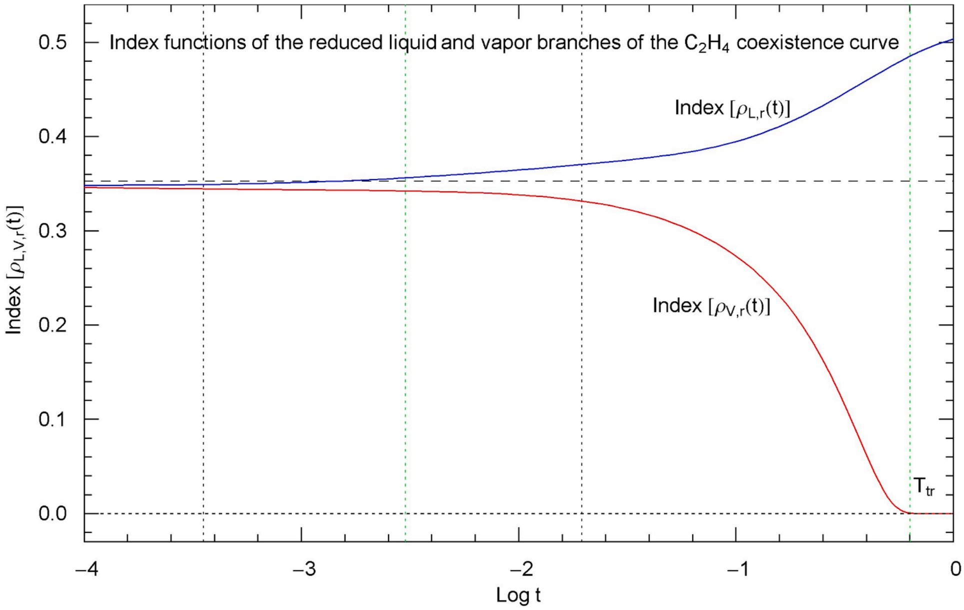

Fig. 12. Index functions (effective exponents) of the reduced liquid and vapor branches of the C_2H_4 coexistence curve. The blue and red solid curves Index$[\rho_{\mathrm{L,r}}(t)]$ and Index$[\rho_{\mathrm{V,r}}(t)]$ show the temperature evolution of the Log−Log slope of the reduced coexistence-curve branches in Fig. 9, cf. Sections 4 and 5. The two vertical black dotted lines indicate the temperature interval covered by data points of Ref. [3] (black filled symbols in Fig. 9) and the vertical green dotted lines the interval covered by data points from Refs. [1,2] (open symbols in Fig. 9). The horizontal dashed line is the common asymptote of the Index curves, representing the constant Index function (scaling exponent) of the asymptotic power law $B_{\mathrm{ord}}t^{\beta}$ (dashed straight line in Fig. 9).

the reduced branches $\rho_{\mathrm{V,r}}(t)$ and $\rho_{\mathrm{L,r}}(t)$ are shown in the lower panels.

Figs. 3, 10 and 17 depict the order parameter $\rho_{\mathrm{ord}}(t) = (\rho_{\mathrm{L}}(t) - \rho_{\mathrm{V}}(t))/2$ and the coexistence-curve diameter $\rho_{\mathrm{dia}}(t) = (\rho_{\mathrm{L}}(t) + \rho_{\mathrm{V}}(t))/2$ (cf. Section 2) of N_2, C_2H_4 and SF_6, respectively, assembled from the regressed branches $\rho_{\mathrm{L}}(t)$ and $\rho_{\mathrm{V}}(t)$ of the coexistence curve, cf. (3.1), (3.2) and Tables 2 and 3. Also depicted are the corresponding data points, obtained by adding or subtracting the experimental densities of the liquid and vapor branches of the coexistence curve, cf. Figs. 1, 8 and 15 and Section 2. The residuals of the data points with respect to $\rho_{\mathrm{ord}}(t)$ and $\rho_{\mathrm{dia}}(t)$ are indicated in the lower panels of Figs. 3, 10 and 17. The asymptotic power-law scaling $\rho_{\mathrm{ord}}(t) \sim B_{\mathrm{ord}}t^{\beta}$ of the order parameter, cf. (2.4) and after (3.3), is indicated by the black dashed straight line (asymptotic to the $\rho_{\mathrm{ord}}(t)$ curve) in the Log−Log coordinates of these figures. The regressed scaling exponent β is listed in Table 2 for each fluid, as well as the amplitude ($B_{\mathrm{ord}} = a$ in Table 2).

Figs. 4, 11 and 18 show the reduced coexistence-curve diameter $\rho_{\mathrm{dia,r}} = \rho_{\mathrm{dia}}(t) - 1$ of N_2, C_2H_4 and SF_6 and the corresponding data points, cf. Section 2. The asymptotic power-law scaling $\rho_{\mathrm{dia,r}} \sim (b_l - b_{\mathrm{v}})t^{\lambda}/2$ of the reduced diameter, cf. after (3.3) and Tables 2

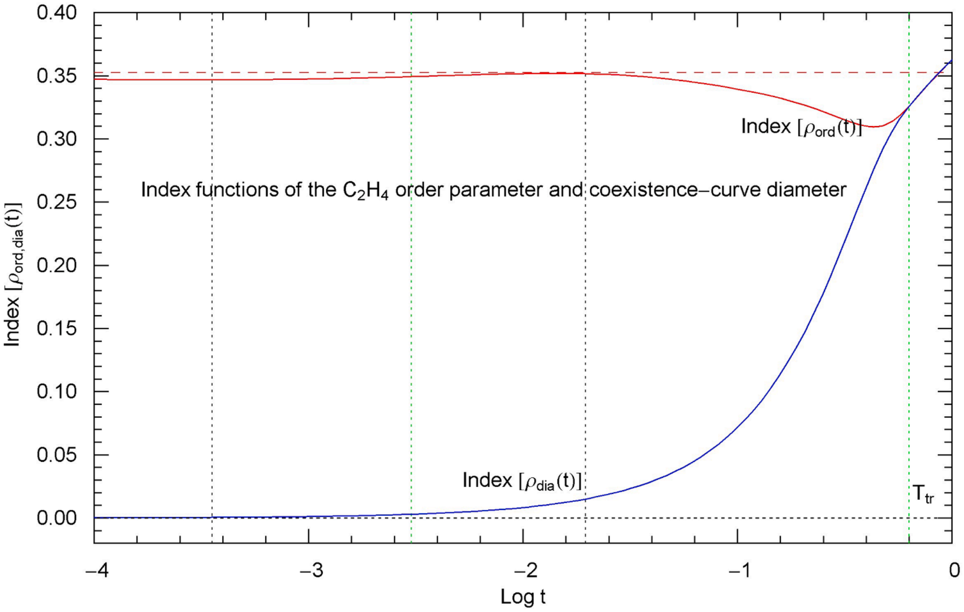

Fig. 13. Index functions (effective exponents) of the order parameter and coexistence-curve diameter of ethylene. The red and blue solid curves show the slope evolution Index[$\rho_{ord}(t)$] and Index[$\rho_{dia}(t)$] of the order parameter and diameter in Fig. 10, cf. Sections 4 and 5. The vertical black dotted lines indicate the temperature interval covered by data points of Ref. [3] (black filled symbols in Fig. 10) and the vertical green dotted lines the interval covered by data points from Refs. [1,2] (open symbols in Fig. 10). The horizontal red dashed line, asymptotically tangent to the Index[$\rho_{ord}(t)$] curve, is the constant Index function Index[$B_{ord}t^{\beta}$] $= \beta$ of the asymptotic order parameter $B_{ord}t^{\beta}$ (dashed straight line in Fig. 10).

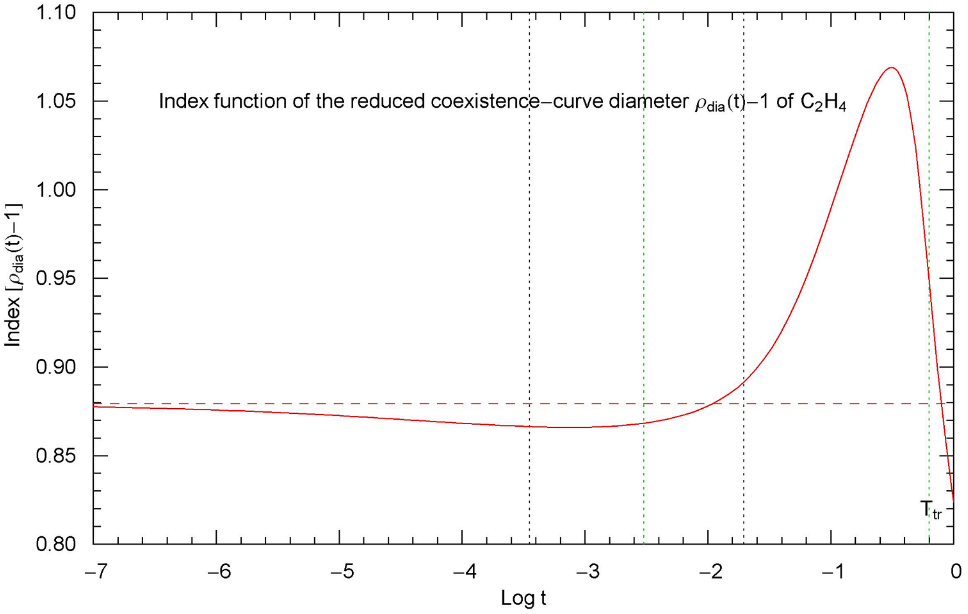

Fig. 14. Index function (effective exponent) of the reduced coexistence-curve diameter of ethylene. Depicted is the Index function Index[$\rho_{dia,r}(t)$] (red solid curve), cf. Sections 4 and 5, of the reduced diameter in Fig. 11, representing the temperature evolution of the Log−Log slope of $\rho_{dia,r}(t)$. The two vertical black dotted lines indicate the temperature interval covered by data points of Ref. [3] (black filled symbols in Fig. 11) and the vertical green dotted lines the interval covered by data points from Refs. [1,2] (open symbols in Fig. 11). The horizontal red dashed line is the asymptote of the Index[$\rho_{dia,r}(t)$] curve, depicting the constant Index function (scaling exponent) of the asymptotic power-law limit of the reduced diameter $\rho_{dia,r}(t)$ (black dashed straight line in Fig. 11), cf. after (3.3) and Section 5.

and 3, is depicted as black dashed straight line asymptotically tangent to the regressed curve $\rho_{dia,r}(t)$. The Log−Log slope of this tangent line is the power-law exponent λ, which is, for all three fluids, noticeably larger than 2β, where β is the scaling exponent of the order parameter mentioned above, cf. Table 2. As discussed in Section 3.1, critical scaling theory predicts the reduced diameter to scale as $\rho_{dia,r}(t) \propto t^{2\beta}$ with $\beta =$ 0.3264 for the 3D Ising universality class, and the next-to-leading order term to scale as $\propto t^{1-\alpha}$, where $\alpha = 0.1101$ is the 3D Ising exponent of the isochoric specific heat, cf. (3.7) and Refs. [12–21,37–39]. The regressed exponent λ is much closer to $1-\alpha = 0.8899$ than $2\beta = 0.6528$, cf. Table 2 and the discussion below. The exponent β of the order parameter in Table 2 is also deviating from the calculated 3D Ising exponent. This can be made more explicit by way of Index functions.

Figs. 5, 12 and 19 show the Index functions representing the

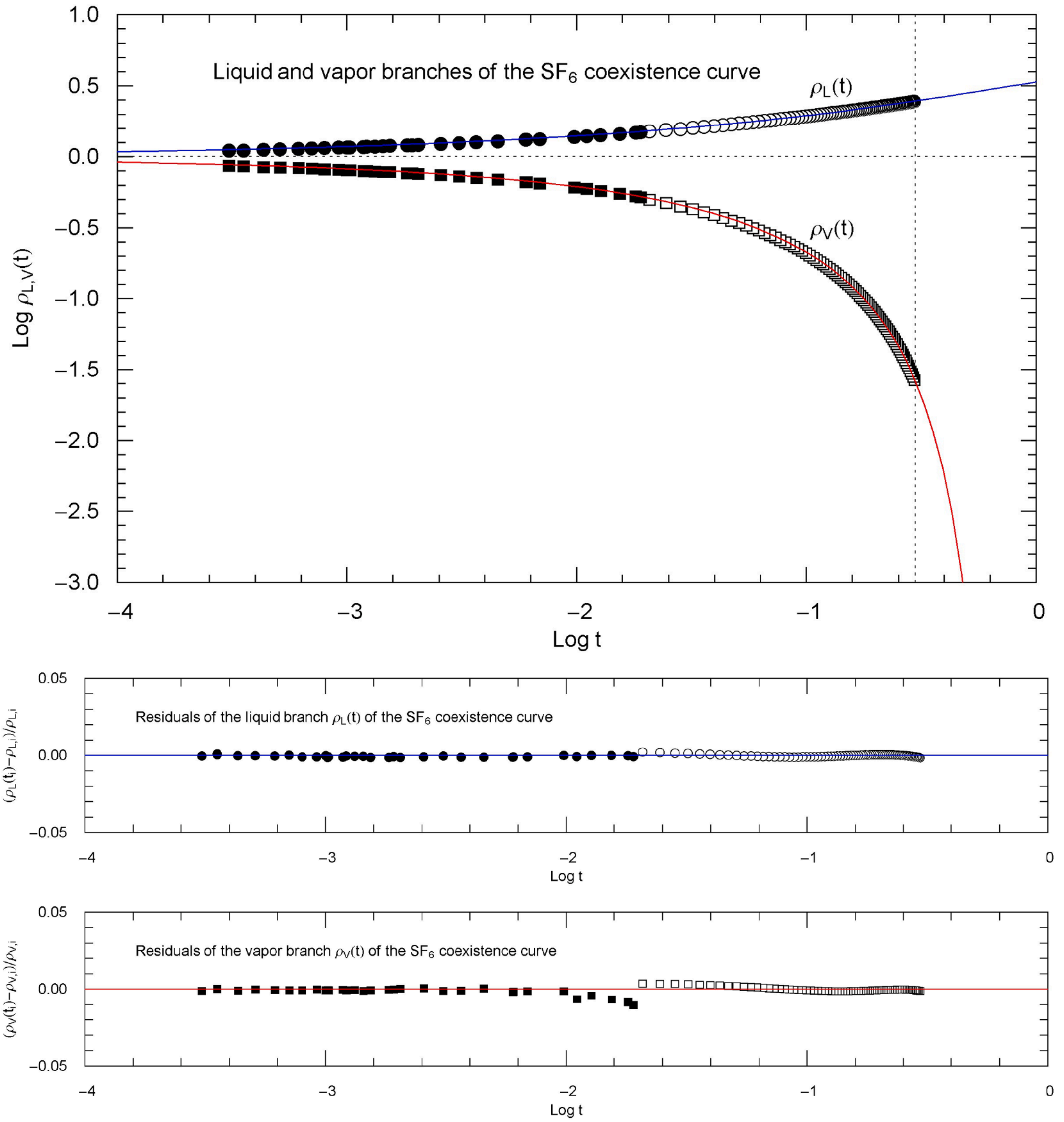

Fig. 15. Coexistence curve of sulfur hexafluoride. Depicted are the liquid and vapor branches $\rho_L(t)$ and $\rho_V(t)$ of the coexistence curve, cf. Sections 2 and 5. The data sets are from Ref. [3] (filled symbols) and Refs. [1,2] (open symbols). The vertical dotted line indicates the SF_6 triple-point temperature, cf. Table 1. The blue and red solid curves show the regressed branches $\rho_L(t)$ and $\rho_V(t)$ in (3.1) and (3.2), with parameters in Tables 2 and 3. Residual plots of the regressed branches are shown in the lower panels.

Log−Log slope (effective exponent, cf. Section 4) of the reduced liquid and vapor branches $\rho_{L,r}(t)$, $\rho_{V,r}(t)$ of the N_2, C_2H_4 and SF_6 coexistence curves (which are depicted in Log−Log coordinates in Figs. 2, 9 and 16). The black dashed horizontal line in Figs. 5, 12 and 19 is the common asymptote of the Index curves $\mathrm{Index}[\rho_{L,r}(t)]$ and $\mathrm{Index}[\rho_{V,r}(t)]$, depicting the constant Index function $\mathrm{Index}[B_{\mathrm{ord}}t^{\beta}] = \beta$ of the critical power-law scaling $B_{\mathrm{ord}}t^{\beta}$ of the two branches, cf. (2.2). (The power law $B_{\mathrm{ord}}t^{\beta}$ is indicated by the black dashed straight line in Figs. 2, 9 and 16, which is the common asymptote of the reduced branches $\rho_{L,r}(t)$ and $\rho_{V,r}(t)$ in these figures.) The Index functions are calculated from the regressed branches, cf. (4.1), and are plotted in Lin-Log coordinates. The two vertical black dotted lines in Figs. 5, 12 and 19 indicate the temperature interval covered by data points of Ref. [3] (depicted by black filled symbols in Figs. 2, 9, and 16). The vertical green dotted lines indicate the interval (extending to the triple point) covered by data points from Refs. [1,2] (open symbols in Figs. 2, 9 and 16). These intervals substantially overlap, except in the case of SF_6 (Fig. 19), where the synthetic data of Refs. [1,2] become incompatible with those of Ref. [3] and have been truncated for that reason. (The synthetic N_2 and C_2H_4 data sets of Ref. [1,2] have also been truncated, as they are known to become inaccurate close to the critical point, cf. Refs. [8–11].)

Figs. 6, 13 and 20 depict the Index functions $\mathrm{Index}[\rho_{\mathrm{ord}}(t)]$ and $\mathrm{Index}[\rho_{\mathrm{dia}}(t)]$ of the order parameter and coexistence-curve diameter of N_2, C_2H_4 and SF_6, respectively (plotted in Log−Log coordinates in Figs. 3, 10 and 17). These Index functions are assembled from the regressed liquid and vapor branches (3.1) and (3.2) of the coexistence curve as outlined in Section 4 and show the temperature evolution of the Log−Log slope (effective exponent) of the order parameter and coexistence-curve diameter. Also depicted is the constant Index function $\mathrm{Index}[B_{\mathrm{ord}}t^{\beta}] = \beta$ (horizontal red dashed line) of the asymptote $B_{\mathrm{ord}}t^{\beta}$ to the order parameter. (The power law $B_{\mathrm{ord}}t^{\beta}$ is shown in Figs. 3, 10 and 17 as black dashed straight line asymptotically tangent to the order parameter $\rho_{\mathrm{ord}}(t)$.) The vertical black and green dotted lines indicate the temperature intervals covered by data points of Ref. [3] and Refs. [1,2] (depicted in Figs. 3, 10, 17), respectively.

Figs. 7, 14 and 21 show the effective exponent $\mathrm{Index}[\rho_{\mathrm{dia,r}}(t)]$ of the reduced coexistence-curve diameter $\rho_{\mathrm{dia,r}}(t) = \rho_{\mathrm{dia}}(t) - 1$ of N_2, C_2H_4 and SF_6 . (The reduced diameter $\rho_{\mathrm{dia,r}}(t)$ is plotted in Figs. 4, 11 and 18).

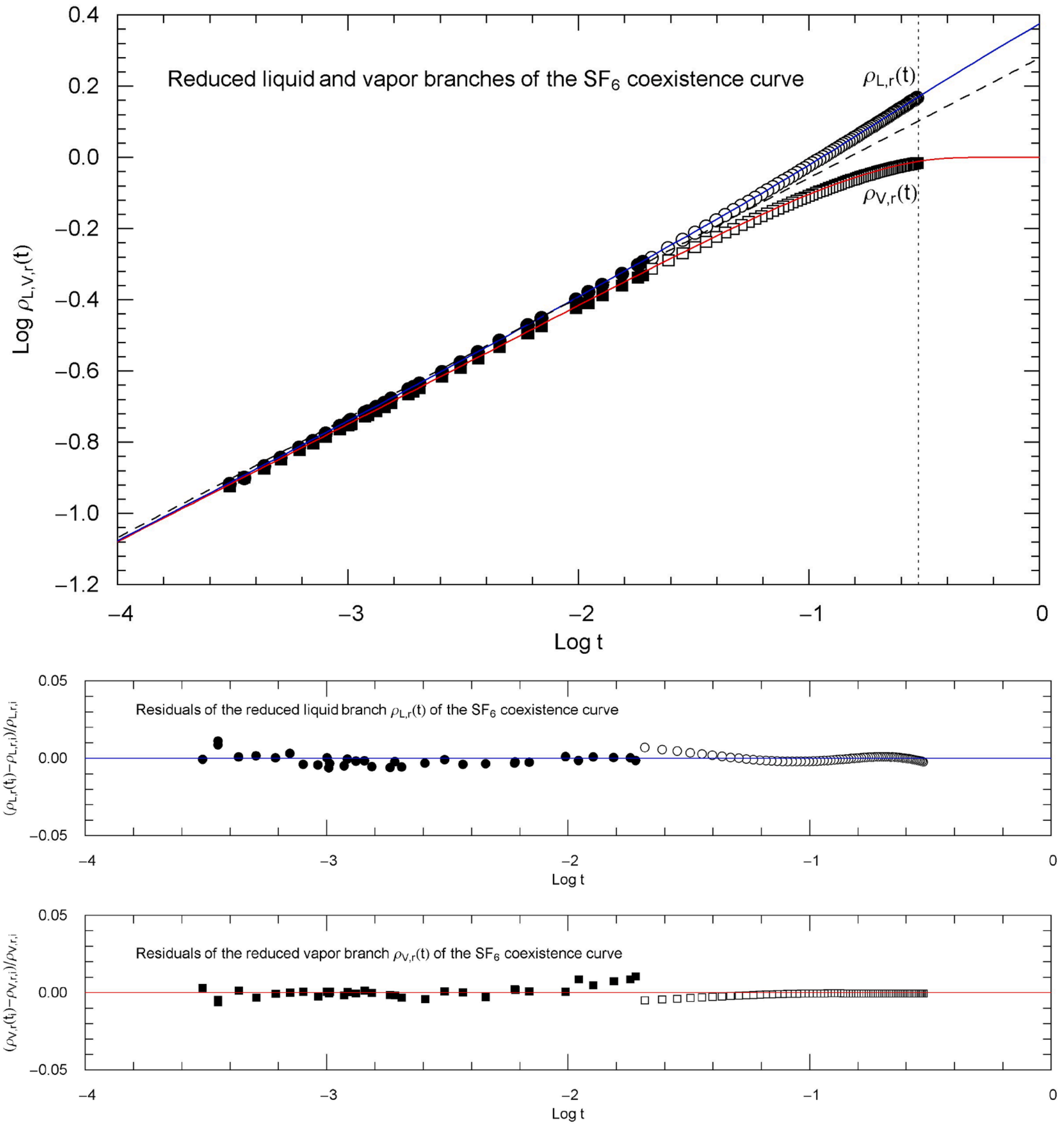

Fig. 16. Reduced liquid and vapor branches of the SF$_6$ coexistence curve. Data points as in Fig. 15. Depicted are the reduced densities $\rho_{\mathrm{L,r}}(t)$ and $\rho_{\mathrm{V,r}}(t)$ (blue and red solid curves), cf. Sections 2 and 5, obtained from the regressed coexistence curve in Fig. 15. The reduced branches converge to a common asymptote, $\rho_{\mathrm{L,r}}(t) \sim \rho_{\mathrm{V,r}}(t) \sim B_{\mathrm{ord}} t^{\beta}$ (black dashed straight line), cf. Sections 2 and 3.1. The SF$_6$ triple-point temperature is indicated by the vertical dotted line. Residual percentage deviations of the regressed curves are shown in the lower panels.

The red dashed horizontal line asymptotic to the Index[$\rho_{\mathrm{dia,r}}(t)$] curve is the constant Index function Index[$(b_l - b_{\mathrm{v}})t^{\lambda}/2$] $= \lambda$ of the critical power law $\rho_{\mathrm{dia,r}} \sim (b_l - b_{\mathrm{v}})t^{\lambda}/2$ of the reduced diameter, cf. after (3.3). (This power law is plotted in Figs. 4, 11 and 18 as black dashed straight line asymptotically tangent to the $\rho_{\mathrm{dia,r}}(t)$ curve.)

It is evident from the Index functions in Figs 7, 14 and 21, that the asymptotic power-law scaling of the reduced diameter (with regressed exponent λ listed in Table 2), cf. after (3.3), is only reached at temperatures extremely close to the critical temperature, $t < 10^{-6}$ ($t = 1 - T/T_{\mathrm{c}}$). In the temperature intervals covered by data points in Figs. 7, 14 and 21, the Log−Log slope (effective exponent) of the reduced diameter varies between 0.86 and 1.08 in the case of nitrogen and ethylene, cf. Figs. 7 and 14, and between 0.77 and 1.05 for SF$_6$, cf. Fig. 21. These intervals thus cover the Log−Log slope of one, as exemplified by the rectilinear diameter rule, and also the slope of $1 - \alpha = 0.8899$, where α is the calculated scaling exponent of the isochoric 3D Ising heat capacity [6], cf. Section 3.1. The slope is varying with temperature and becomes constant (and thus a power-law index, λ in this case) only in the asymptotic scaling limit. As mentioned, the ideal power-law scaling limits of N$_2$, C$_2$H$_4$ and SF$_6$ are attained at reduced temperatures $t < 10^{-6}$, which are by two orders beyond the experimental temperature range located outside the $t < 10^{-4}$ interval. The asymptotic power-law scaling $\rho_{\mathrm{dia,r}}(t) \propto t^{2\beta}$ of the reduced diameter with exponent $2\beta = 0.6528$ predicted by the Yang−Yang anomaly (see below) for the 3D Ising universality class is not visible in the Index plots of Figs. 7, 14 and 21.

As the ideal power-law scaling predicted by critical scaling theory only happens in an extremely narrow temperature interval, perturbative ascending series expansions have been used in experimental papers to extend the ideal power-law scaling regime to a more accessible temperature range. For instance, in the case of the order parameter, a truncated series $\rho_{\mathrm{ord}} \sim B_{\mathrm{ord}} t^{\beta}(1 + B_{\mathrm{ord},1} t^{\Delta} + \cdots)$ is employed, cf., e.g., Refs. [27–30], where $\Delta = 0.523$ is a universal correction-to-scaling exponent, cf. Ref. [6]. Such expansions are believed to be valid at most within the interval $|T/T_{\mathrm{c}} - 1| < 0.1$. (The observation of power-law slopes in the interval $|T/T_{\mathrm{c}} - 1| < 10^{-4}$ is also impeded by gravitational stratification and impurities distorting the power-law slopes [47–49].) These series expansions are only applicable in an

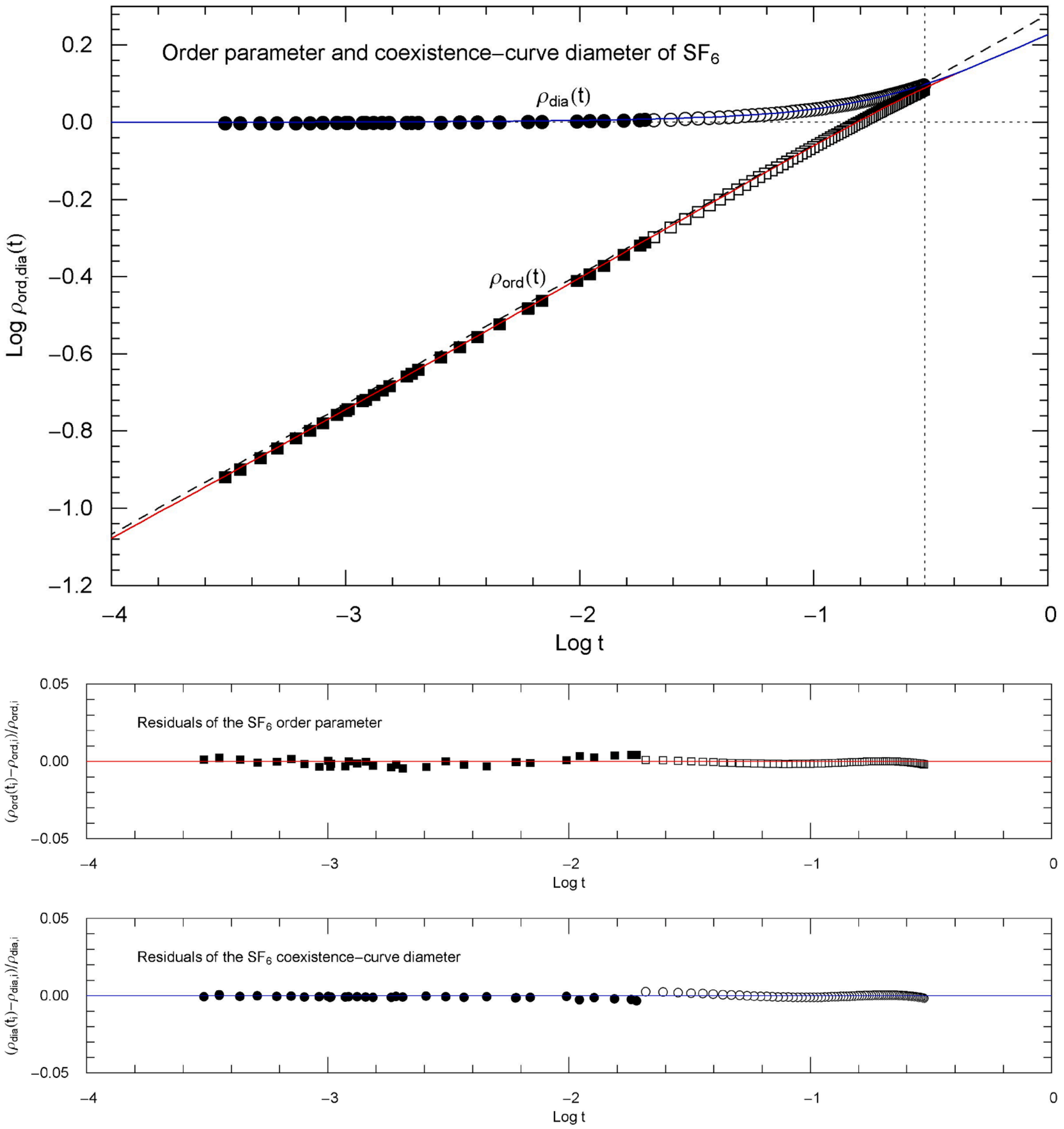

Fig. 17. Order parameter and coexistence-curve diameter of sulfur hexafluoride. Depicted are the liquid−vapor order parameter $\rho_{\mathrm{ord}}(t)$ (red solid curve) and the coexistence-curve diameter $\rho_{\mathrm{dia}}(t)$ (blue solid curve) assembled from the regressed liquid and vapor branches of the coexistence curve in Fig. 15, cf. Sections 2 and 5. The black dashed straight line is the asymptote of the order parameter, representing the critical power-law scaling $\rho_{\mathrm{ord}}(t) \sim B_{\mathrm{ord}} t^{\beta}$, cf. Section 3.1. The vertical dotted line indicates the triple-point temperature, cf. Table 1. Residual plots of the order parameter and diameter are shown in the lower panels.

interval where power-law scaling with small correction terms still prevails. In contrast, the nonlinear regression explained in Section 3.2 is global, treating critical and subcritical data sets on equal footing and covering a temperature range of which the critical regime is only a small fraction.

When performing least-squares fits with the above series expansion, it is customary to fix the exponents at the calculated 3D Ising values $\beta = 0.3264$ and $\Delta = 0.523$ and to infer the series coefficients by linear χ^2 regression. A small χ^2 is then regarded as evidence for the consistency of the data set with critical scaling theory and for the universality of the 3D Ising exponents.

The exponent β of a nitroethane + 3-methylpentane mixture was estimated as 0.366 ± 0.012, cf. Ref. [4], and of an n-heptane + nitrobenzene mixture as 0.367 ± 0.006, cf. Ref. [5]. Regarding liquid alkali metals, β exponents of 0.355 ± 0.01 for Cs and 0.360 ± 0.01 for Rb were obtained in Ref. [7], also consistently above the quoted 3D Ising exponent. Perhaps it is more prudent to regard the Ising critical exponents as somewhat idealized, and to allow for deviations in real systems. After all, the fact that the critical compressibility factor appears as universal constant in the standard cubic equations of state (van der Waals, Redlich−Kwong and Peng−Robinson, cf., e.g., Ref. [50]) does not preclude either that this factor weakly varies in reality from fluid to fluid. See also Refs. [51–53], where the effect of shear flows on the critical parameters of colloid−polymer mixtures was studied, and Ref. [54] and references therein, where varying critical exponents were observed in ferromagnetic crystals.

The β values listed in Table 2, derived by allowing this exponent to float in the least-squares regression, slightly differ for the fluids examined (0.3353 ± 0.0018 for N_2, 0.3524 ± 0.0014 for C_2H_4, and 0.3366 ± 0.0022 for SF_6) and deviate from the calculated 3D Ising exponent $\beta = 0.3264$, although by a smaller margin than the β values quoted above. The error bounds were estimated from the saturated vapor density of the respective fluid, as explained at the end of Section 3.2. The regressed exponent λ (0.854 ± 0.008 for N_2, 0.879 ± 0.008 for C_2H_4, and 0.886 ± 0.013 for SF_6, cf. Table 2) is close to the 3D Ising exponent $1 - \alpha = 0.8899$ in each case. This exponent λ determines the leading-order

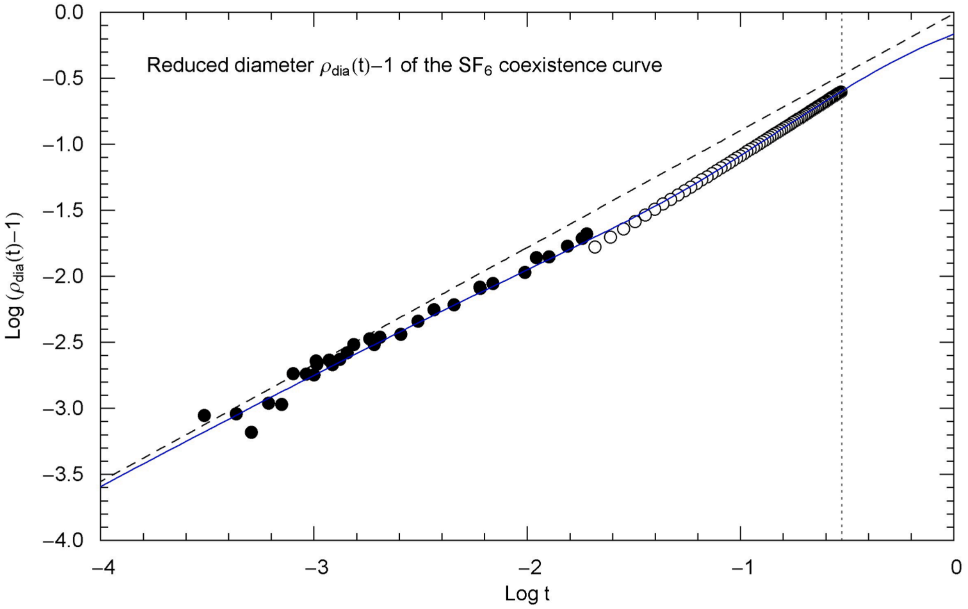

Fig. 18. Reduced coexistence-curve diameter of sulfur hexafluoride. The blue solid curve depicts the reduced diameter $\rho_{\mathrm{dia,r}}(t)$ calculated from the regressed liquid and vapor branches $\rho_{\mathrm{L}}(t)$ and $\rho_{\mathrm{V}}(t)$ in Fig. 15, cf. Sections 2 and 5. The black dashed straight line is the asymptote of $\rho_{\mathrm{dia,r}}(t)$, depicting the power-law scaling of the reduced diameter, cf. after (3.3) and Section 5. The vertical dotted line indicates the triple-point temperature, cf. Table 1.

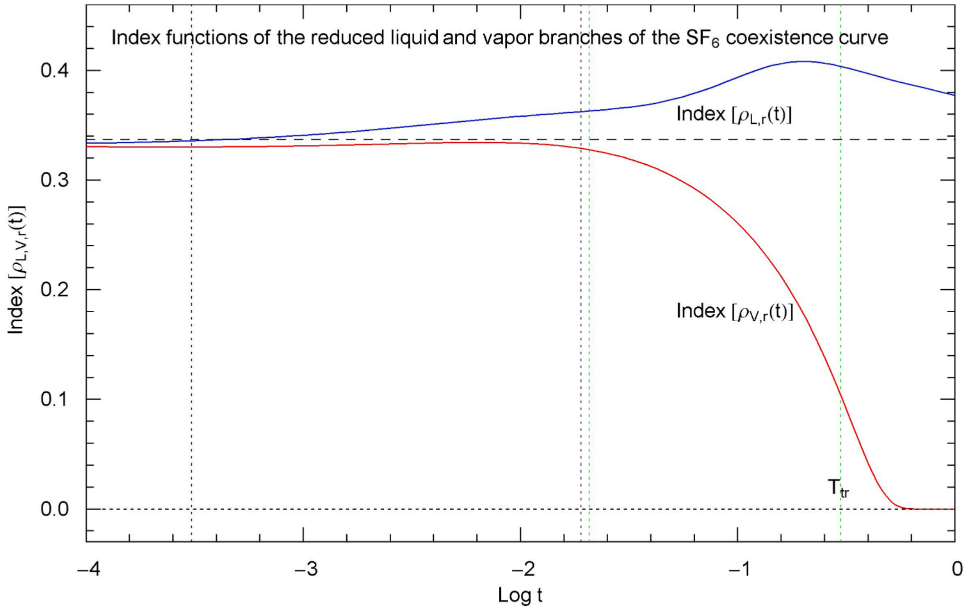

Fig. 19. Index functions (effective exponents) of the reduced liquid and vapor branches of the SF_6 coexistence curve. The blue and red solid curves Index$[\rho_{\mathrm{L,r}}(t)]$ and Index$[\rho_{\mathrm{V,r}}(t)]$ show the temperature evolution of the Log−Log slope of the reduced coexistence-curve branches in Fig. 16, cf. Sections 4 and 5. The two vertical black dotted lines indicate the temperature interval covered by data points of Ref. [3] (black filled symbols in Fig. 16) and the vertical green dotted lines the interval covered by data points from Refs. [1,2] (open symbols in Fig. 16). The horizontal dashed line is the common asymptote of the Index curves, representing the constant Index function Index$[B_{\mathrm{ord}}t^{\beta}] = \beta$ of the asymptotic power law $B_{\mathrm{ord}}t^{\beta}$ (dashed straight line in Fig. 16).

scaling of the reduced diameter, cf. after (3.3). In particular, we did not find evidence for the Yang−Yang anomaly (i.e. divergence of the second temperature derivative of the chemical potential), cf. Ref. [12], manifested in critical scaling theory by a leading $t^{2\beta}$ power law of the reduced diameter, cf. (3.7), with 3D Ising exponent $2\beta = 0.6528$. By the way, the authors of Ref. [3], who used the same data sets in the critical regime and tried linear regression with truncated series expansions and fixed 3D Ising exponents, arrived at the conclusion that the leading-order scaling exponent of the reduced diameter is $1 - \alpha$, fairly close to the regressed λ exponents of N_2, C_2H_4 and SF_6 quoted above.

We also performed the regression of the vapor and fluid branches (3.1) and (3.2) of the coexistence curve with exponents β and $\lambda = 1 - \alpha$ kept fixed at the calculated 3D Ising values. The regressed parameters and goodness-of-fit parameters (determination coefficient R^2 and standard error SE, cf. Section 3) in this case are listed in Tables 4 and 5. (In fact, the parameters in these tables were used as initial values for the regression with varying exponents β and λ, cf. Tables 2 and 3.)

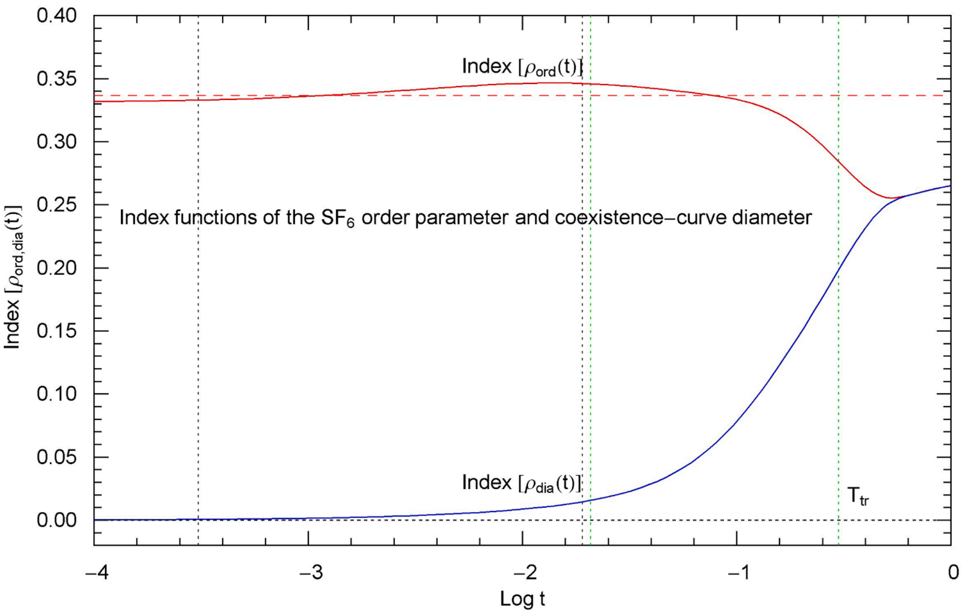

Fig. 20. Index functions (effective exponents) of the order parameter and coexistence-curve diameter of sulfur hexafluoride. The red and blue solid curves show the Log−Log slope evolution Index$[\rho_{ord}(t)]$ and Index$[\rho_{dia}(t)]$ of the order parameter and diameter in Fig. 17, cf. Sections 4 and 5. The two vertical black dotted lines indicate the temperature interval covered by data points of Ref. [3] (black filled symbols in Fig. 17) and the vertical green dotted lines the interval covered by data points from Refs. [1,2] (open symbols in Fig. 17). The horizontal red dashed line, asymptotically tangent to the Index$[\rho_{ord}(t)]$ curve, is the constant Index function Index$[B_{ord}t^{\beta}] = \beta$ of the asymptotic order parameter $B_{ord}t^{\beta}$ (dashed straight line in Fig. 17).

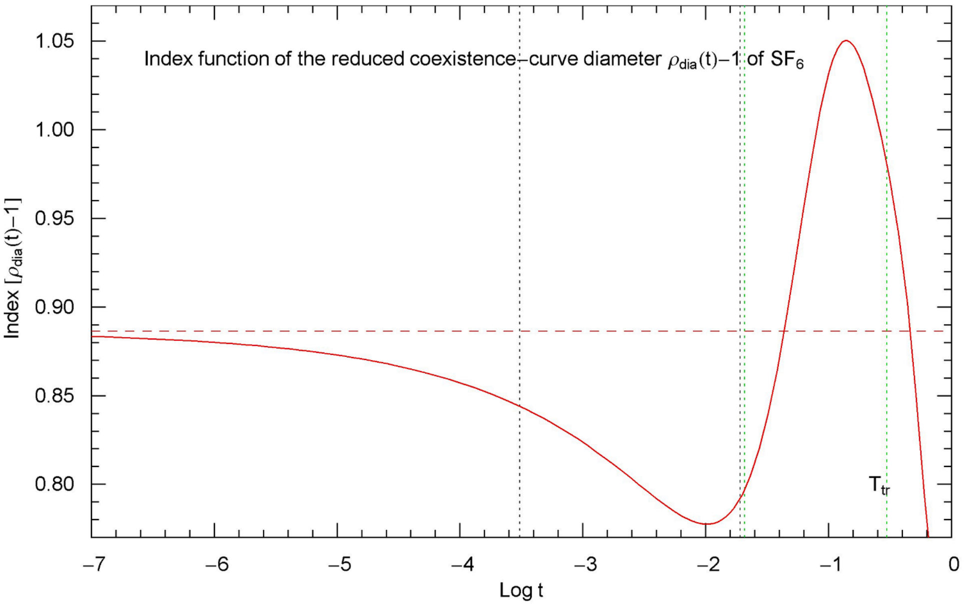

Fig. 21. Index function (effective exponent) of the reduced coexistence-curve diameter of sulfur hexafluoride. Depicted is the Index function Index$[\rho_{dia,r}(t)]$ (red solid curve), cf. Sections 4 and 5, of the reduced diameter in Fig. 18, representing the temperature evolution of the Log−Log slope of $\rho_{dia,r}(t)$. The two vertical black dotted lines indicate the temperature interval covered by data points of Ref. [3] (black filled symbols in Fig. 18) and the vertical green dotted lines the interval covered by data points from Refs. [1,2] (open symbols in Fig. 18). The horizontal red dashed line is the asymptote of the Index$[\rho_{dia,r}(t)]$ curve, depicting the constant Index function (scaling exponent) of the asymptotic power-law limit of the reduced diameter $\rho_{dia,r}(t)$ (black dashed straight line in Fig. 18), cf. after (3.3) and Section 5.

Comparing the χ^2, R^2 and SE values in Tables 2 and 4 (for vapor densities) and also in Tables 3 and 5 (for liquid densities), we find, unsurprisingly, that the least-squares fits with 3D Ising exponents imposed are less accurate than those with β and λ as fitting parameters. Even so, since the χ^2, R^2 and SE values in Tables 4 and 5 are still good, one can defensibly argue that the 3D Ising exponents are consistent with the data sets. On the other hand, allowing the exponents to float in the regression, the 3D Ising β exponent is not recovered within the error bounds of the regressed parameters (as pointed out above), so that this consistency falls short of proof. The latter requires to extract the exponents from the data sets alone, without invoking the calculated 3D Ising exponents as input in the least-squares regression.

6. Conclusion

The purpose of this paper was the empirical modeling of the coexistence curve over the entire temperature range from the critical point to the triple point and to extrapolate the saturated vapor curve regressed in this interval to zero temperature. The vapor−liquid order parameter and the coexistence-curve diameter were obtained by subtracting or adding the regressed liquid and vapor branches of the curve, cf. Section 2.

We discussed the coexistence curve of three molecular fluids, nitrogen, ethylene, and SF_6. These fluids were selected since there are, in each case, precision data sets available, densely covering the temperature interval from the triple point into the $10^{-4} < 1 - T/T_c < 10^{-3}$ decade. In the least-squares regression, we avoided any calculated input from critical scaling and renormalization-group theory, in particular we did not assume the power-law scaling exponents of the order parameter and the reduced diameter to be those of the 3D Ising model, which is frequently done when regressing coexistence curves from empirical data sets.

Since the aim was the global modeling of the coexistence curve in the interval $T_{tr} \le T \le T_c$, of which the critical scaling regime (discussed in greater detail in Section 5) covers only a tiny fraction, we also avoided the use of perturbative expansions, and performed the regression of the liquid and vapor branches of the coexistence curve with elementary closed-form distributions, that is broken power-law densities and Weibull exponentials, cf. (3.1) and (3.2). These distributions turned out to be sufficiently adaptable to accurately describe the coexistence curve of the mentioned fluids, as is evident from the residual plots of the least-squares fits depicted in Figs. 1,2,8,9,15,16, which show relative deviations of below one percent over the entire experimental data range.

Notation

The listed symbols are introduced in the indicated sections.

Section 2

T_c, ρ_c, P_c, V_c	critical temperature, molar density, pressure and molar volume
$\rho_L(t), \rho_V(t)$	liquid and vapor branches of the coexistence curve (molar densities normalized with ρ_c)
T_{tr}	triple-point temperature
$t = 1 - T/T_c$	reduced temperature in the subcritical interval $0 \le t \le 1$
$(t_i, \rho_{L,i})_{i=1,\ldots,N}, (t_i, \rho_{V,i})_{i=1,\ldots,N}$	data points of the coexistence-curve branches $\rho_L(t)$, $\rho_V(t)$
$\rho_{L,r}(t) = \rho_L - 1, \rho_{V,r}(t) = 1 - \rho_V$	reduced liquid and vapor branches of the coexistence curve
$\rho_{ord}(t), \rho_{dia}(t)$	order parameter and coexistence-curve diameter
B_{ord}, β	critical amplitude and exponent of the order parameter $\rho_{ord}(t)$
$(t_i, \rho_{ord,i})_{i=1,\ldots,N}, (t_i, \rho_{dia,i})_{i=1,\ldots,N}$	data points of the order parameter and coexistence-curve diameter
$\rho_{dia,r}(t) = \rho_{dia} - 1$	reduced coexistence-curve diameter
$(t_i, \rho_{dia,r,i})_{i=1,\ldots,N}$	data points of the reduced coexistence-curve diameter

Section 3.1

$a = B_{ord}, b_v$ and $\beta, \lambda, \gamma_v, \eta_v$	amplitudes and exponents parametrizing the vapor branch $\rho_V(t)$ of the coexistence curve
$a = B_{ord}, b_l, d_l$ and $\beta, \lambda, \delta_l, \kappa_l$	amplitudes and exponents parametrizing the liquid branch $\rho_L(t)$ of the coexistence curve
$t_{tr} = 1 - T_{tr}/T_c$	reduced temperature at the triple point
α	critical exponent of the isochoric heat capacity

Section 3.2

χ^2_V, χ^2_L	least-squares functionals of the vapor and liquid branches of the coexistence curve
r_c	scale factor in the least-squares functionals
χ^2_{V+L}	least-squares functional for the simultaneous regression of the liquid and vapor branches of the coexistence curve
R^2	coefficient of determination
SE	standard error of a least-squares fit

Section 4

$\mathrm{Index}[\rho(t)]$	Index functional defining the Log–Log slope (effective exponent) of a density $\rho(t)$

Declaration of Competing Interest

The author declares that he has no known competing financial interests or personal relationships that could have appeared to influence the work reported in this paper.

Data availability

The data tables of Ref. [3] were used for the critical scaling regime. The URLs of the machine-readable data used in the subcritical regime above the triple point are indicated in Refs. [1,2].

Acknowledgments

My thanks to two anonymous referees for their suggestions and useful comments, which have greatly helped to improve an earlier draft of this paper.

References

[1] E.W. Lemmon, I.H. Bell, M.L. Huber, M.O. McLinden, NIST Standard Reference Data-base 23, Reference Fluid Thermodynamic and Transport Properties-REFPROP, Version 10.0, National Institute of Standards and Technology, Gaithersburg, 2018, https://doi.org/10.18434/T4/1502528.

[2] E.W. Lemmon, M.O. McLinden, D.G. Friend, NIST chemistry WebBook. NIST Standard Reference Database 69, 2023. https://webbook.nist.gov/chemistry/fluid/.

[3] M.W. Pestak, R.E. Goldstein, M.H.W. Chan, J.R. de Bruyn, D.A. Balzarini, N. W. Ashcroft, Three-body interactions, scaling variables, and singular diameters in the coexistence curves of fluids, Phys. Rev. B 36 (1987) 599–614, https://doi.org/10.1103/PhysRevB.36.599.

[4] P. Venkatesu, Effect of polymer chain in coexisting liquid phases by refractive index measurements, J. Chem. Phys. 123 (2005), 024902, https://doi.org/10.1063/1.1953576.

[5] N. Fameli, D.A. Balzarini, Coexistence curve of the *n*-heptane + nitrobenzene mixture near its consolute point measured by an optical method, Phys. Rev. B 75 (2007), 064203, https://doi.org/10.1103/PhysRevB.75.064203.

[6] S. El-Showk, M.F. Paulos, D. Poland, S. Rychkov, D. Simmons-Duffin, A. Vichi, Solving the 3d Ising model with the conformal bootstrap II. *c*-Minimization and precise critical exponents, J. Stat. Phys. 157 (2014) 869–914, https://doi.org/10.1007/s10955-014-1042-7.

[7] S. Jüngst, B. Knuth, F. Hensel, Observation of singular diameters in the coexistence curves of metals, Phys. Rev. Lett. 55 (1985) 2160–2163, https://doi.org/10.1103/PhysRevLett.55.2160.

[8] R. Span, E.W. Lemmon, R.T. Jacobsen, W. Wagner, A. Yokozeki, A reference equation of state for the thermodynamic properties of nitrogen for temperatures from 63.151 to 1000 K and pressures to 2200 MPa, J. Phys. Chem. Ref. Data 29 (2000) 1361–1433, https://doi.org/10.1063/1.1349047.

[9] R. Span, E.W. Lemmon, R.T. Jacobsen, W. Wagner, A reference quality equation of state for nitrogen, Int. J. Thermophys. 19 (1998) 1121–1132, https://doi.org/10.1023/A:1022689625833.

[10] J. Smukala, R. Span, W. Wagner, A new equation of state for ethylene covering the fluid region for temperatures from the melting line to 450 K at pressures up to 300 MPa, J. Phys. Chem. Ref. Data 29 (2000) 1053–1122, https://doi.org/10.1063/1.1329318.

[11] C. Guder, W. Wagner, A reference equation of state for the thermodynamic properties of sulfur hexafluoride (SF_6) for temperatures from the melting line to 625 K and pressures up to 150 MPa, J. Phys. Chem. Ref. Data 38 (2009) 33–94, https://doi.org/10.1063/1.3037344.

[12] Y.C. Kim, M.E. Fisher, Singular coexistence-curve diameters: experiments and simulations, Chem. Phys. Lett. 414 (2005) 185–192, https://doi.org/10.1016/j.cplett.2005.07.105.

[13] J. Wang, M.A. Anisimov, Nature of vapor−liquid asymmetry in fluid criticality, Phys. Rev. E 75 (2007), 051107, https://doi.org/10.1103/PhysRevE.75.051107.

[14] I.M. Abdulagatov, N.G. Polikhronidi, T.J. Bruno, R.G. Batyrova, G.V. Stepanov, Measurements of the isochoric heat capacity, the critical point (T_c, ρ_c) and vapor–liquid coexistence curve (T_s, ρ_s) of high-purity toluene near the critical point, Fluid Phase Equilibr. 263 (2008) 71–84, https://doi.org/10.1016/j.fluid.2007.09.023.

[15] L.M. Radzhabova, G.V. Stepanov, I.M. Abdulagatov, K.A. Shakhbanov, Experimental study of the isochoric heat capacity of isobutanol in the critical and

supercritical regions, J. Supercrit. Fluids 63 (2012) 115–132, https://doi.org/10.1016/j.supflu.2011.11.017.
[16] I.M. Abdulagatov, N.G. Polikhronidi, R.G. Batyrova, Yang−Yang critical anomaly strength parameter from the direct two-phase isochoric heat capacity measurements near the critical point, Fluid Phase Equilibr. 415 (2016) 144–157, https://doi.org/10.1016/j.fluid.2016.01.041.
[17] Z. Hao, Z. Cui, T. Yin, P. Zheng, J. Zhao, W. Shen, Liquid–liquid phase equilibria of ionic liquid solutions in the critical region: 1-methyl-3-octylimidazolium tetrafluoroborate with 1-pentanol or 1-hexanol, Fluid Phase Equilibr. 380 (2014) 58–66, https://doi.org/10.1016/j.fluid.2014.07.036.
[18] C. Xu, X. Wang, Z. Chen, T. Yin, W. Shen, Measurements of heat capacities and turbidities for binary mixtures {water + 2,6-dimethylpyridine} and {water, or heavy water + 2,6-dimethylpiperidine} in the critical regions, Fluid Phase Equilibr. 409 (2016) 361e368, https://doi.org/10.1016/j.fluid.2015.10.027.
[19] X. Tao, T. Yin, C. Xu, W. Shen, Critical phenomena in {bromobenzene + 1-hexyl-3-methylimidazolium bis(trifluoromethylsulfonyl)imide} binary solution, Fluid Phase Equilibr. 415 (2016) 184e192, https://doi.org/10.1016/j.fluid.2016.02.011.
[20] A. Drozd-Rzoska, S.J. Rzoska, J. Kalabiński, Impact of pressure on low-molecular weight near-critical mixtures of limited miscibility, ACS Omega 5 (32) (2020) 20141–20152, https://doi.org/10.1021/acsomega.0c01772.
[21] S.J. Rzoska, J. Kalabiński, A. Drozd-Rzoska, Critical concentration in binary mixtures of limited miscibility, Fluid Phase Equilibr. 540 (2021), 112979, https://doi.org/10.1016/j.fluid.2021.112979.
[22] J.S. Kouvel, M.E. Fisher, Detailed magnetic behavior of nickel near its Curie point, Phys. Rev. 136 (1964) A1626–A1632, https://doi.org/10.1103/PhysRev.136.A1626.
[23] J.V. Sengers, J.G. Shanks, Experimental critical-exponent values for fluids, J. Stat. Phys. 137 (2009) 857–877, https://doi.org/10.1007/s10955-009-9840-z.
[24] R. Tomaschitz, Modeling electrical resistivity and particle fluxes with multiply broken power-law distributions, Eur. Phys. J. Plus 136 (2021) 629, https://doi.org/10.1140/epjp/s13360-021-01542-5.
[25] R. Tomaschitz, Multiparameter equation of state for classical and quantum fluids, J. Supercrit. Fluids 181 (2022), 105491, https://doi.org/10.1016/j.supflu.2021.105491.
[26] R. Tomaschitz, Phenomenological high-pressure equation of state for nitrogen, methane, methanol, carbon dioxide, and helium, Int. J. Thermophys. 43 (2022) 130, https://doi.org/10.1007/s10765-022-03034-9.
[27] J.R. de Bruyn, D.A. Balzarini, Critical behavior of hydrogen, Phys. Rev. B 39 (1989) 9243–9251, https://doi.org/10.1103/PhysRevB.39.9243.
[28] U. Närger, D.A. Balzarini, Universal critical amplitude ratios in CHF_3, Phys. Rev. B 39 (1989) 9330–9335, https://doi.org/10.1103/PhysRevB.39.9330.
[29] M.W. Pestak, M.H.W. Chan, Equation of state of N_2 and Ne near their critical points. Scaling, corrections to scaling, and amplitude ratios, Phys. Rev. B 30 (1984) 274–288, https://doi.org/10.1103/PhysRevB.30.274.
[30] D. Balzarini, O.G. Mouritsen, Universal ratio of correction-to-scaling amplitudes for Xe, Phys. Rev. A 28 (1983) 3515–3519, https://doi.org/10.1103/PhysRevA.28.3515.
[31] E.M. Apfelbaum, V.S. Vorob'ev, The wide-range method to construct the entire coexistence liquid−gas curve and to determine the critical parameters of metals, J. Phys. Chem. B 119 (2015) 11825–11832, https://doi.org/10.1021/acs.jpcb.5b06336.
[32] E.A. Vazquez, J.L. Alvarez, M.L. Japas, Liquid−vapor coexistence curve and critical point of sodium, revisited, Fluid Phase Equilibr. 443 (2017) 14–22, https://doi.org/10.1016/j.fluid.2017.03.030.
[33] J.B. McDonald, Y.J. Xu, A generalization of the beta distribution with applications, J. Econom. 66 (1995) 133–152, https://doi.org/10.1016/0304-4076(94)01612-4.
[34] R. Tomaschitz, Multiply broken power-law densities as survival functions: an alternative to Pareto and lognormal fits, Physica A 541 (2020), 123188, https://doi.org/10.1016/j.physa.2019.123188.
[35] R. Tomaschitz, Isobaric heat capacity of carbon dioxide at critical pressure: singular thermodynamic functions as multiply broken power laws, Physica A 611 (2023), 128421, https://doi.org/10.1016/j.physa.2022.128421.
[36] N.L. Johnson, S. Kotz, N. Balakrishnan, Continuous Univariate Distributions, 2nd ed., vol. 1, Wiley, New York, 1994.
[37] I.M. Abdulagatov, J.W. Magee, N.G. Polikhronidi, R.G. Batyrova, Yang–Yang critical anomaly, in: E. Wilhelm, T. Letcher (Eds.), Enthalpy and Internal Energy: Liquids, Solutions and Vapours, Royal Society of Chemistry, London, 2018.
[38] N.G. Polikhronidi, R.G. Batyrova, J.W. Magee, I.M. Abdulagatov, Isochoric heat capacity of near- and supercritical benzene and derived thermodynamic properties, J. Mol. Liq. 313 (2020), 113204, https://doi.org/10.1016/j.molliq.2020.113204.
[39] S.M. Rasulov, I.A. Isaev, M. Dzida, I.M. Abdulagatov, $P\rho T$ and liquid-gas phase transition properties (P_s, ρ_s, T_s) of binary *n*-hexane + methyl octanoate mixture near the critical point of pure *n*-hexane, Fluid Phase Equilibr. 556 (2022), 113382, https://doi.org/10.1016/j.fluid.2022.113382.
[40] Wolfram Research, Inc., Mathematica,® Version 13.2, Champaign, IL, 2023, https://www.wolfram.com/mathematica/.
[41] T.O. Kvålseth, Cautionary note about R^2, Am. Stat. 39 (1985) 279–285, https://doi.org/10.1080/00031305.1985.10479448.
[42] J. Weiner, K.H. Langley, N.C. Ford Jr., Experimental evidence for a departure from the law of the rectilinear diameter, Phys. Rev. Lett. 32 (1974) 879–881, https://doi.org/10.1103/PhysRevLett.32.879.
[43] P.H. Richter, Estimating errors in least-squares fitting, TDA Progress Report 42–122 (1995), https://ipnpr.jpl.nasa.gov/progress_report/42-122/122E.pdf.
[44] R. Tomaschitz, Isobaric heat capacity of classical and quantum fluids: extending experimental data sets into the critical scaling regime, Eur. Phys. J. Plus 138 (2023) 457, https://doi.org/10.1140/epjp/s13360-023-04006-0.
[45] J.B. McDonald, Some generalized functions for the size distribution of income, Econometrica 52 (1984) 647–665, https://doi.org/10.2307/1913469.
[46] J. Esteban, Income-share elasticity and the size distribution of income, Int. Econ. Rev. 27 (1986) 439–444, https://doi.org/10.2307/2526515.
[47] N. Kurzeja, Th. Tielkes, W. Wagner, The nearly classical behavior of a pure fluid on the critical isochore very near the critical point under the influence of gravity, Int. J. Thermophys. 20 (1999) 531–561, https://doi.org/10.1023/A:1022657121329.
[48] M. Barmatz, I. Hahn, J.A. Lipa, R.V. Duncan, Critical phenomena in microgravity: past, present, and future, Rev. Mod. Phys. 79 (2007) 1–52, https://doi.org/10.1103/RevModPhys.79.1.
[49] M.R. Moldover, J.V. Sengers, R.W. Gammon, R.J. Hocken, Gravity effects in fluids near the gas−liquid critical point, Rev. Mod. Phys. 51 (1979) 79–99, https://doi.org/10.1103/RevModPhys.51.79.
[50] R. Tomaschitz, Effective Hamiltonians and empirical fluid equations of state, Fluid Phase Equilibr. 496 (2019) 80–92, https://doi.org/10.1016/j.fluid.2019.05.014.
[51] M.P. Lettinga, H. Wang, J.K. Dhont, Microstructural response of a near-critical colloid-polymer mixture to shear flow, Phys. Rev. E 70 (2004), 061405, https://doi.org/10.1103/PhysRevE.70.061405.
[52] H. Wang, M.P. Lettinga, J.K. Dhont, Microstructure of a near-critical colloidal dispersion under stationary shear flow, J. Phys. Condens. Matter 14 (2002) 7599–7615, https://doi.org/10.1088/0953-8984/14/33/304.
[53] D. Guu, J.K. Dhont, M.P. Lettinga, Dispersions and mixtures of particles with complex architectures in shear flow, Eur. Phys. J. Spec. Top. 222 (2013) 2739–2755, https://doi.org/10.1140/epjst/e2013-02055-2.
[54] N. Khan, P. Sarkar, A. Midya, P. Mandal, P.K. Mohanty, Continuously varying critical exponents beyond weak universality, Sci. Rep. 7 (2017) 45004, https://doi.org/10.1038/srep45004.